Article

Cell

A Neural Circuit for the Suppression of Pain by a Competing Need State

Graphical Abstract

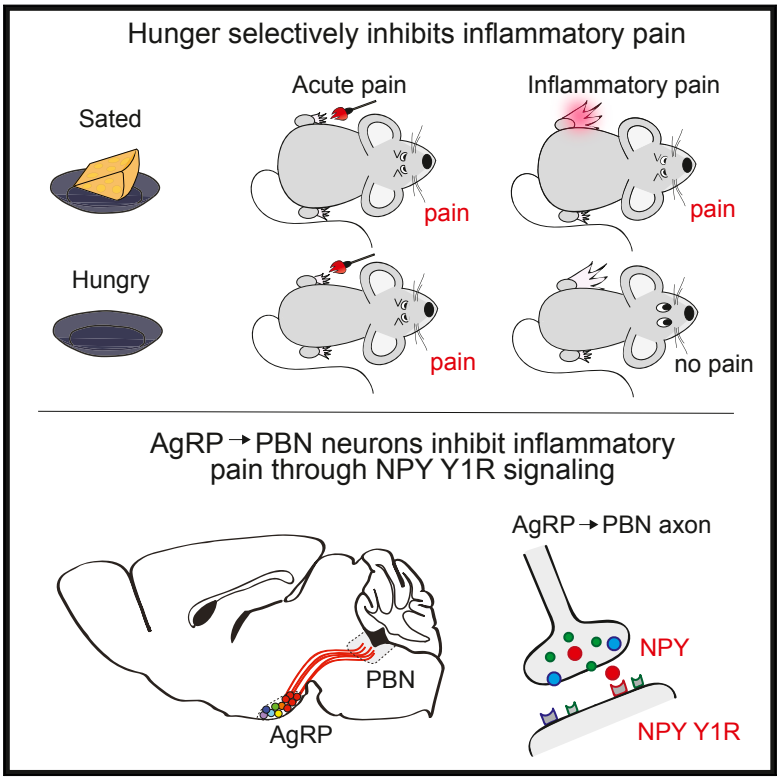

Highlights

- Hunger attenuates inflammatory pain without influencing acute pain responses
- Hunger-sensitive AgRP neurons projecting to the PBN suppress inflammatory pain
- Neuropeptide Y signaling in the PBN attenuates inflammatory pain during hunger

Authors

Amber L. Alhadeff, Zhenwei Su, Elen Hernandez, ..., Adam W. Hantman, Bart C. De Jonghe, J. Nicholas Betley

Correspondence

jnbetley@sas.upenn.edu

In Brief

Hunger suppresses responses to pain through an AgRP/NPY circuit.

Alhadeff et al., 2018, Cell *173*, 140–152
March 22, 2018
https://doi.org/10.1016/j.cell.2018.02.057

CellPress

Cell

Article

A Neural Circuit for the Suppression of Pain by a Competing Need State

Amber L. Alhadeff,[1] Zhenwei Su,[1] Elen Hernandez,[1] Michelle L. Klima,[1] Sophie Z. Phillips,[1] Ruby A. Holland,[2] Caiying Guo,[3] Adam W. Hantman,[3] Bart C. De Jonghe,[2] and J. Nicholas Betley[1,4,*]

[1]Department of Biology, University of Pennsylvania, Philadelphia, PA 19104, USA
[2]Department of Biobehavioral Health Sciences, University of Pennsylvania, Philadelphia, PA 19104, USA
[3]Janelia Research Campus, Howard Hughes Medical Institute, Ashburn, VA 20147, USA
[4]Lead Contact
*Correspondence: jnbetley@sas.upenn.edu
https://doi.org/10.1016/j.cell.2018.02.057

SUMMARY

Hunger and pain are two competing signals that individuals must resolve to ensure survival. However, the neural processes that prioritize conflicting survival needs are poorly understood. We discovered that hunger attenuates behavioral responses and affective properties of inflammatory pain without altering acute nociceptive responses. This effect is centrally controlled, as activity in hunger-sensitive agouti-related protein (AgRP)-expressing neurons abrogates inflammatory pain. Systematic analysis of AgRP projection subpopulations revealed that the neural processing of hunger and inflammatory pain converge in the hindbrain parabrachial nucleus (PBN). Strikingly, activity in AgRP → PBN neurons blocked the behavioral response to inflammatory pain as effectively as hunger or analgesics. The anti-nociceptive effect of hunger is mediated by neuropeptide Y (NPY) signaling in the PBN. By investigating the intersection between hunger and pain, we have identified a neural circuit that mediates competing survival needs and uncovered NPY Y1 receptor signaling in the PBN as a target for pain suppression.

INTRODUCTION

Survival depends on fulfilling salient needs in a changing environment. Formative behavioral observations highlighted the remarkable ability of individuals across species to adaptively respond to dynamic physiological and environmental challenges (Pavlov and Fol'bort, 1926; Tinbergen, 1951). Given these insights, it is surprising that the neural and molecular mechanisms governing the prioritization of adaptive behaviors remain elusive. While great strides have been made in understanding how individual need states such as hunger, thirst, fear, and pain are signaled in the brain, relatively little is known about how the brain prioritizes such needs.

Pain is a natural response to injury, but long-term inflammation and associated pain can be maladaptive. While acute pain is reflexive in that it is triggered by activation of primary sensory neurons (i.e., nociceptors) in the periphery, inflammatory pain is mediated at least in part by central mechanisms (Coderre et al., 1990). From this perspective, targeting central nociceptive pathways may be an effective way to selectively reduce inflammatory pain while leaving intact adaptive responses to acute pain. Because persistent pain remains a major public health burden that is not well-controlled by current analgesics (Loeser, 2012), identifying endogenous mechanisms that specifically reduce the inflammatory response to injury may provide strategies for the design of effective pain therapies.

As a unique approach to identify neural circuits that regulate pain, we sought to explore competing need states that affect nociception. The response to pain is typically an adaptive mechanism that protects organisms against dangerous stimuli. However, as other physiological needs such as hunger increase, behavior must shift from avoiding bodily injury to fulfilling other immediate needs. Interactions between competing need states have been reported (e.g., acute stressors such as inescapable footshock, cold-water swims, or caloric deprivation can produce short-term analgesia) (Bodnar et al., 1977, 1978b; Hamm and Lyeth, 1984; Hargraves and Hentall, 2005; LaGraize et al., 2004). Additionally, hunger has been shown to influence adaptive behavioral responses to fear and anxiety (Burnett et al., 2016; Jikomes et al., 2016; Padilla et al., 2016). We reasoned that individuals must prioritize the most acute threat to survival and behave accordingly. To explore the behavioral, neural, and molecular mechanisms that rank survival needs, we examined the bidirectional interaction between hunger and different modalities of pain.

Here, we found that hunger selectively inhibits both the behavioral response and affective properties of inflammatory pain. Because neurons responsive to hunger are well-characterized (Sternson and Eiselt, 2017), they provide an entry point to examine the neural circuit intersection of hunger and pain. We discovered that hypothalamic agouti-related protein (AgRP)-expressing neurons that project to the hindbrain parabrachial nucleus (PBN) selectively inhibit responses to inflammatory pain. The analgesic effect of hunger on inflammatory pain is mediated by neuropeptide Y (NPY) signaling on NPY Y1 receptors in the PBN. We further show that acute thermal, but not inflammatory, pain inhibits the activity of AgRP neurons, demonstrating that central mechanisms prioritize the most salient threat. Taken together, our data demonstrate that AgRP neurons mediate

the interaction between hunger and pain and have uncovered PBN NPY Y1 receptor signaling as a target for analgesia.

RESULTS

Hunger Selectively Attenuates Responses to Inflammatory Pain

To understand how competing survival signals are prioritized, we first explored how 24-hr food deprivation influences the behavioral response to pain induced by either chemical (formalin), thermal (52°C hotplate), or mechanical (Von Frey filament) insults (Figures 1A, 1H, and 1J) (Bodnar et al., 1978a; Hamm and Lyeth, 1984; Hargraves and Hentall, 2005; LaGraize et al., 2004). Formalin paw injection is a reliable and widely used model of nociception with high face validity when tested with analgesic drugs (Hunskaar and Hole, 1987). Formalin induces distinct acute (0–5 min) and long-term inflammatory (15–45 min) phases of pain (Dubuisson and Dennis, 1977), while responses to a hotplate or Von Frey filaments are acute and transient. We discovered that 24-hr food deprivation attenuated the duration (Figures 1B–1D) and frequency (Figure 1E) of inflammatory paw licking after injection of a noxious chemical stimulus, similar to the effect of an anti-inflammatory painkiller (Hunskaar and Hole, 1987) (Figures S1A–S1E). Conversely, food deprivation had no effect on the acute phase response to formalin injection (Figures 1F and 1G) or the response to acute thermal (Figures 1H and 1I) or mechanical (Figures 1J and 1K) pain, unlike an opioid painkiller (Figures S1F–S1H). These data demonstrate that hunger selectively blocks inflammatory phase pain responses.

To determine whether hunger influences inflammation-induced sensitization to different modalities of pain, we next induced a persistent inflammatory response in the paw via injection of complete Freund's adjuvant (CFA) (Marchand et al., 2005). After paw injection of CFA, mice exhibit sensitization to both mechanical (Figures 2A, 2B, and 2E) and thermal (Figures 2G and 2H) stimuli. The sensitization to both of these stimuli is abolished in food-restricted mice (Figures 2C, 2D, 2F, and 2I), suggesting that hunger reduces inflammation-induced sensitization to thermal and mechanical pain. Taken together, these data suggest that hunger is a powerful suppressant of inflammatory pain response.

Pain results in both behavioral responses as well as negative affect, the latter of which has been modeled in rodents using classic conditioning paradigms (Deyama et al., 2007; Johansen and Fields, 2004). We first investigated how hunger influences the affective properties of pain by examining whether hunger attenuates a condition placed avoidance normally associated with inflammatory pain (Figure 3A). We found that *ad libitum*-fed mice exhibited a conditioned place avoidance of cues previously paired with formalin-induced inflammatory pain (Figures 3B–3D). This post-conditioning avoidance was abolished in animals that were food-restricted during conditioning (Figures 3B–3D), a result that was independent of changes in locomotor activity (Figures 3E and 3F). This result is not likely due to a hunger-induced deficit in associative learning, given that food-restricted mice learn to avoid contexts associated with other aversive stimuli as effectively as *ad libitum*-fed mice (Figure 3G). Similar to the attenuation of a formalin-conditioned place avoidance, we found that hunger also attenuated formalin-induced immobility (Figure 3H). Together, these data suggest that hunger attenuates measures of pain-induced negative affect, in addition to behavioral responses to inflammatory pain.

AgRP Neurons Specifically Inhibit Inflammatory Pain

Formalin paw injection leads to paw inflammation in food-deprived mice (Figures S1I and S1J), suggesting central mechanisms may mediate the interaction between hunger and inflammatory pain. Neural circuits activated by hunger are well-characterized (Sternson and Eiselt, 2017). In particular, neurons that co-express AgRP, gamma-aminobutyric acid (GABA), and NPY (referred to as AgRP neurons) are critical regulators of food intake (Luquet et al., 2005). AgRP neuron inhibition in hungry mice reduces food intake (Krashes et al., 2011), while activation of AgRP neurons in sated mice robustly increases food intake (Aponte et al., 2011; Krashes et al., 2011). Photostimulation of mice expressing channelrhodopsin-2 (ChR2) in AgRP neurons ($AgRP^{ChR2}$) dramatically reduced both formalin-induced inflammatory phase pain responses (Figures 4A–4D and S2A–S2C) and CFA-induced nociceptive sensitization (Figures 4E, 4F, and S2F–S2H) relative to responses of GFP-expressing control mice ($AgRP^{GFP}$). This effect was specific to inflammatory pain as activating AgRP neurons did not influence acute phase chemical or thermal pain responses (Figures S2D, S2E, S2I, and S2J) nor responses to control saline paw injections (Figures S2K–S2M). Initiating AgRP neuron stimulation during an ongoing pain response inhibited paw licking within minutes (Figures 4G and 4H). This indicates that AgRP neuron activity rapidly mediates a behavioral switch and does not rely on long-term activity of AgRP neurons that may entrain a single behavioral state. To test whether AgRP neuron activity is sufficient to suppress inflammatory pain, we chemogenetically inhibited AgRP neurons during hunger. Food-deprived mice expressing inhibitory designer receptors exclusively activated by designer drugs (DREADDs, hM4D) in AgRP neurons ($AgRP^{hM4D+}$) significantly reduce food intake relative to littermate controls ($AgRP^{hM4D-}$) following injection of the designer ligand clozapine-N-oxide (CNO) (Figure 4I), as previously described (Krashes et al., 2011). Inhibition of AgRP neurons significantly reduced the protective effect of hunger on inflammatory pain (Figures 4J–4L). Thus, AgRP neuron activity during hunger is both necessary and sufficient to suppress inflammatory pain responses without affecting acute pain responses, recapitulating the behavioral interaction observed in hunger and identifying a neural mechanism for the suppression of inflammatory pain.

AgRP → PBN Neurons Specifically Inhibit Inflammatory Pain

Given that hunger suppresses longer-term inflammatory pain responses, we next sought to identify brain regions where hunger and nociceptive information converge. Several brain regions innervated by AgRP neurons are also activated by formalin paw injection and implicated in nociception (Baulmann et al., 2000). To explore potential brain regions targeted by AgRP neurons that mediate inflammatory pain, we performed a formalin paw injection in *ad libitum*-fed mice and quantified neurons

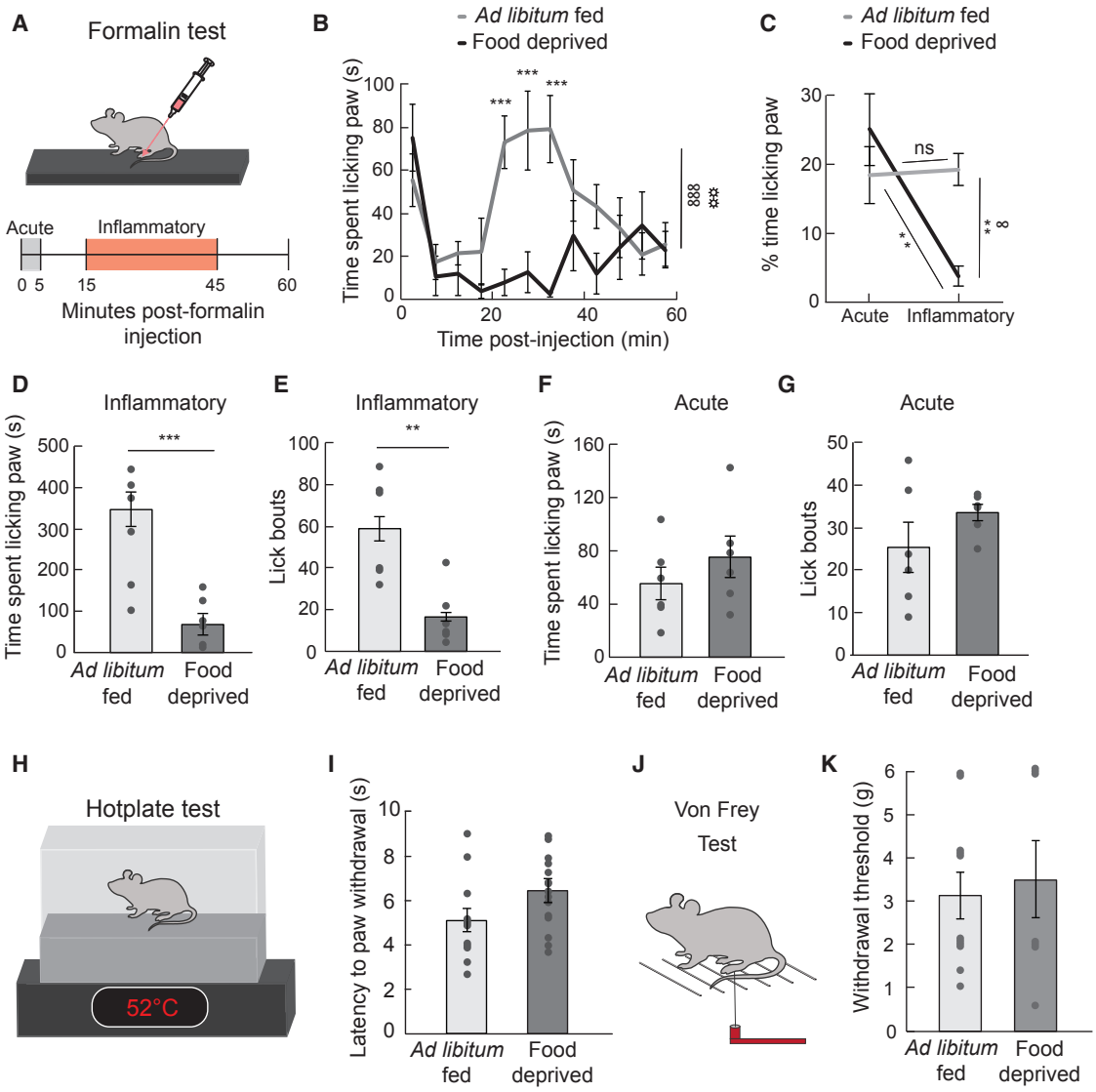

Figure 1. Hunger Attenuates Response to Inflammatory Pain

(A) Experimental design (formalin test): paw injection of 2% formalin was administered at 0 min; time spent licking paw was measured for 60 min and quantified during the acute phase (0–5 min) and the inflammatory phase (15–45 min).

(B) Time spent licking paw following formalin injection displayed in 5-min time bins in *ad libitum*-fed (n = 6) and 24-hr food-deprived (n = 6) mice (two-way repeated-measures ANOVA, $p < 0.001$).

(C) % time spent paw licking during acute and inflammatory phases of formalin test (two-way repeated-measures ANOVA, $p < 0.05$).

(D) Time spent paw licking during the inflammatory phase of formalin test in *ad libitum*-fed and 24-hr food-deprived mice (unpaired t test, $p < 0.001$).

(E) Lick bouts during the inflammatory phase of formalin test in *ad libitum*-fed and 24-hr food-deprived mice (unpaired t test, $p < 0.01$).

(F) Time spent paw licking during the acute phase of formalin test in *ad libitum*-fed and 24-hr food-deprived mice (unpaired t test, p = not significant [ns]).

(G) Lick bouts during the acute phase of formalin test in *ad libitum*-fed and 24-hr food-deprived mice (unpaired t test, p = ns).

(H) Experimental design (hotplate test): latency to withdraw paw from 52°C hotplate was measured.

(I) Latency to withdraw paw in *ad libitum*-fed (n = 12) versus 24-hr food-deprived (n = 14) mice during hotplate test (unpaired t test, p = ns).

(J) Experimental design (Von Frey): paw withdrawal from Von Frey filaments was measured.

(K) Withdrawal threshold (Von Frey filament at which mouse responded to >50% of trials) in *ad libitum*-fed (n = 11) versus 24-hr food-deprived (n = 7) mice (unpaired t test, p = ns). Data are expressed as mean ± SEM, ns $p > 0.05$, t tests and post hoc comparisons: *$p < 0.05$, **$p < 0.01$, ***$p < 0.001$; ANOVA interaction: ∞$p < 0.05$, ∞∞∞$p < 0.001$; ANOVA main effect of group: ☼☼$p < 0.01$.

See also Figure S1 and Table S1.

directly under AgRP axons that expressed the immediate early gene Fos. The number of neurons expressing Fos protein was increased in the terminal projection fields of several AgRP neuron target regions following formalin paw injection compared to mice who received saline or no injection (Figures 5A, 5B and S3A).

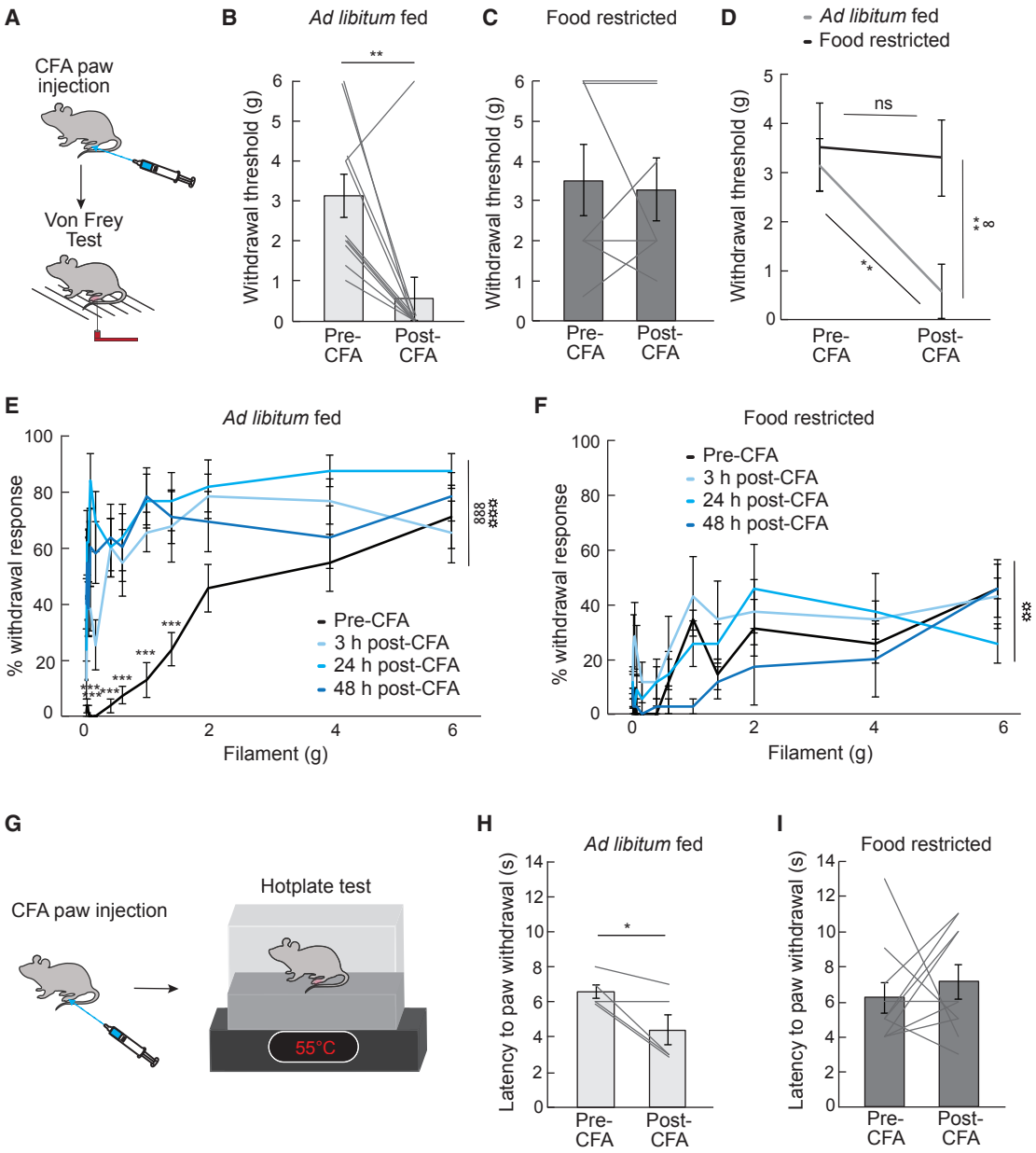

Figure 2. Hunger Attenuates Inflammation-Induced Sensitization to Mechanical and Thermal Pain

(A) Experimental design (complete Freund's adjuvant [CFA] and Von Frey test): CFA was injected in the plantar surface of the hindpaw after a baseline Von Frey test. Mice were subjected again to a Von Frey test 3 hr, 24 hr, and 48 hr post-CFA injection.

(B) Withdrawal threshold (Von Frey filament at which mouse responded to >50% of trials) in *ad libitum*-fed mice (n = 11) before and 24 hr post-CFA injection (paired t test, $p < 0.01$).

(C) Withdrawal threshold in food-restricted mice (n = 7) before and 24 hr post-CFA injection (paired t test, p = ns).

(D) Withdrawal threshold in *ad libitum*-fed (n = 11) and food-restricted mice (n = 7) before and 24 hr post-CFA injection (two-way repeated-measures ANOVA, $p < 0.05$).

(E) Percentage withdrawal from Von Frey filaments before and 3 hr, 24 hr, and 48 hr post-CFA injection in *ad libitum*-fed mice (n = 11, two-way repeated-measures ANOVA, $p < 0.001$).

(F) Percentage withdrawal from Von Frey filaments before and 3 hr, 24 hr, and 48 hr post-CFA injection in food-restricted mice (n = 7, two-way repeated-measures ANOVA, p = ns).

(G) Experimental design (CFA and hotplate test): mice were injected with CFA after a baseline hotplate test. Mice were subjected again to a hotplate test 3 hr, 24 hr, and 48 hr post-CFA injection.

(H) Latency to paw withdrawal from hotplate in *ad libitum*-fed mice (n = 5) before and 48 hr post-CFA injection (paired t test, $p < 0.05$).

(legend continued on next page)

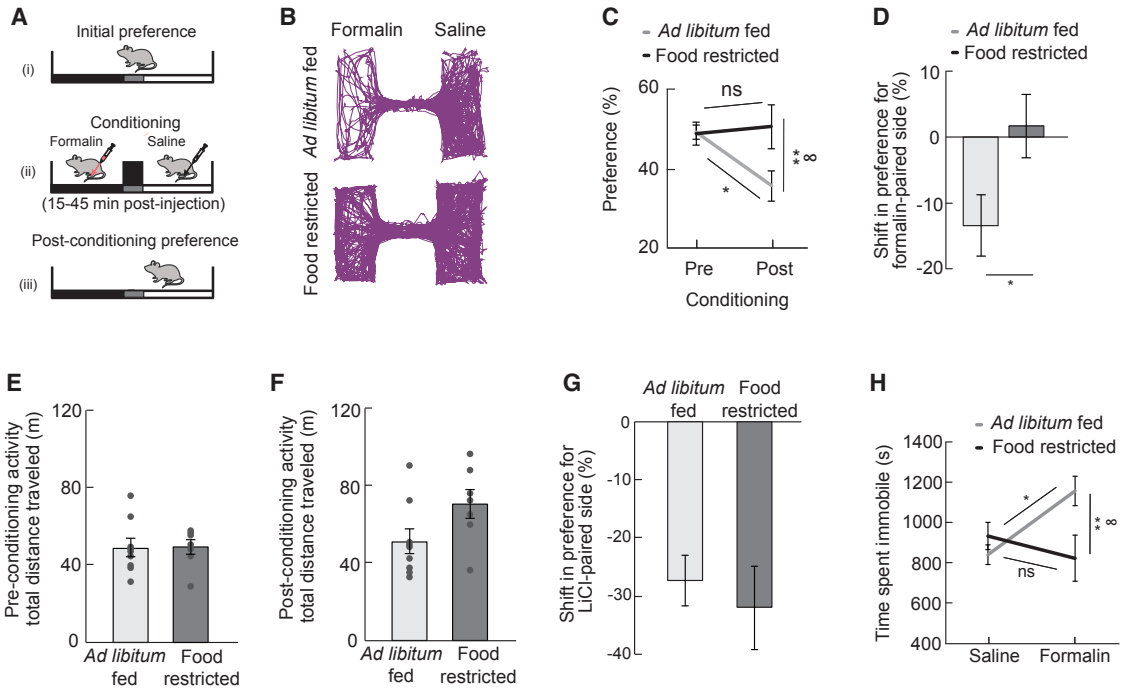

Figure 3. Hunger Attenuates Negative Affective Components of Pain

(A) Experimental design (conditioned place avoidance [CPA]): one side of a two-sided chamber was paired with the inflammatory phase following formalin paw injection in either *ad libitum*-fed or food-restricted mice for 4 days and the post-conditioning preference was measured in replete animals.

(B) Representative traces of locations of mice following formalin CPA.

(C) Preference for formalin-paired side before and after conditioning in *ad libitum*-fed (n = 9) and food-restricted (n = 7) mice (two-way repeated-measures ANOVA, $p < 0.05$).

(D) Shift in preference for formalin-paired side in *ad libitum*-fed and food-restricted mice (unpaired t test, $p < 0.05$).

(E and F) Mice in *ad libitum*-fed (n = 9) and food-restricted (n = 7) groups exhibit similar locomotor activity both before (E) and after (F) CPA to inflammatory phase pain (unpaired t tests, p = ns).

(G) Shift in preference for lithium chloride-paired side in *ad libitum*-fed and food-restricted mice (unpaired t test, p = ns).

(H) Time spent immobile in *ad libitum*-fed and 24-hr food-deprived mice during inflammatory phase following formalin injection (n = 7–10/group, two-way ANOVA, $p < 0.05$). Data are expressed as mean ± SEM, ns $p > 0.05$, t tests and post hoc comparisons: *$p < 0.05$, **$p < 0.01$; ANOVA interaction: ∞ $p < 0.05$.

See also Table S1.

Because the anatomical data suggested that multiple AgRP target regions may be involved in the transmission of inflammatory pain, we performed a systematic analysis of the function of each AgRP neuron projection subpopulation. Taking advantage of the one-to-one architecture of AgRP neuron projections (Figure S3C) (Betley et al., 2013), we activated individual AgRP projection subpopulations in *ad libitum*-fed mice and assessed behavioral responses to acute and inflammatory formalin-induced pain (Figures 5C and S3B). Although AgRP subpopulations that project to the bed nuclei of the stria terminals (BNST), paraventricular thalamic nucleus (PVT), paraventricular hypothalamic nucleus (PVH), and the lateral hypothalamus (LH) are sufficient to evoke food intake (Figure S3D) (Betley et al., 2013), we found that optogenetic activation of each of these discrete subpopulations does not reduce the behavioral response to acute or inflammatory formalin-induced pain (Figures 5D–5F and S3E). Other AgRP projection subpopulations, such as those that project to the periaqueductal gray (PAG), central nucleus of the amygdala (CeA), and parabrachial nucleus (PBN) are not sufficient to drive food intake when stimulated (Figure S3D) (Betley et al., 2013), raising the hypothesis that these populations are involved in more nuanced aspects of feeding, such as the ability to suppress pain to facilitate food-seeking behavior. We found that activation of AgRP projections to the PBN virtually eliminates inflammatory phase pain responses (Figures 5D, 5E, and S3E) without affecting responses to acute chemical (Figure 5F) or thermal (Figure 5G) pain. The suppression of inflammatory pain by AgRP → PBN stimulation is not likely due to off target effects since prolonged stimulation does not reduce the acute response to formalin-induced pain (Figure S3F) or locomotor

(I) Latency to paw withdrawal from hotplate in food-restricted mice (n = 10) before and 48 hr post-CFA injection (paired t test, p = ns). Data are expressed as mean ± SEM, ns $p > 0.05$, t tests and post hoc comparisons: *$p < 0.05$, **$p < 0.01$, ***$p < 0.001$; ANOVA interaction: ∞ $p < 0.05$, ∞ ∞ ∞ $p < 0.001$; ANOVA main effect of drug: ☼☼$p < 0.01$, ☼☼☼$p < 0.001$.

See also Table S1.

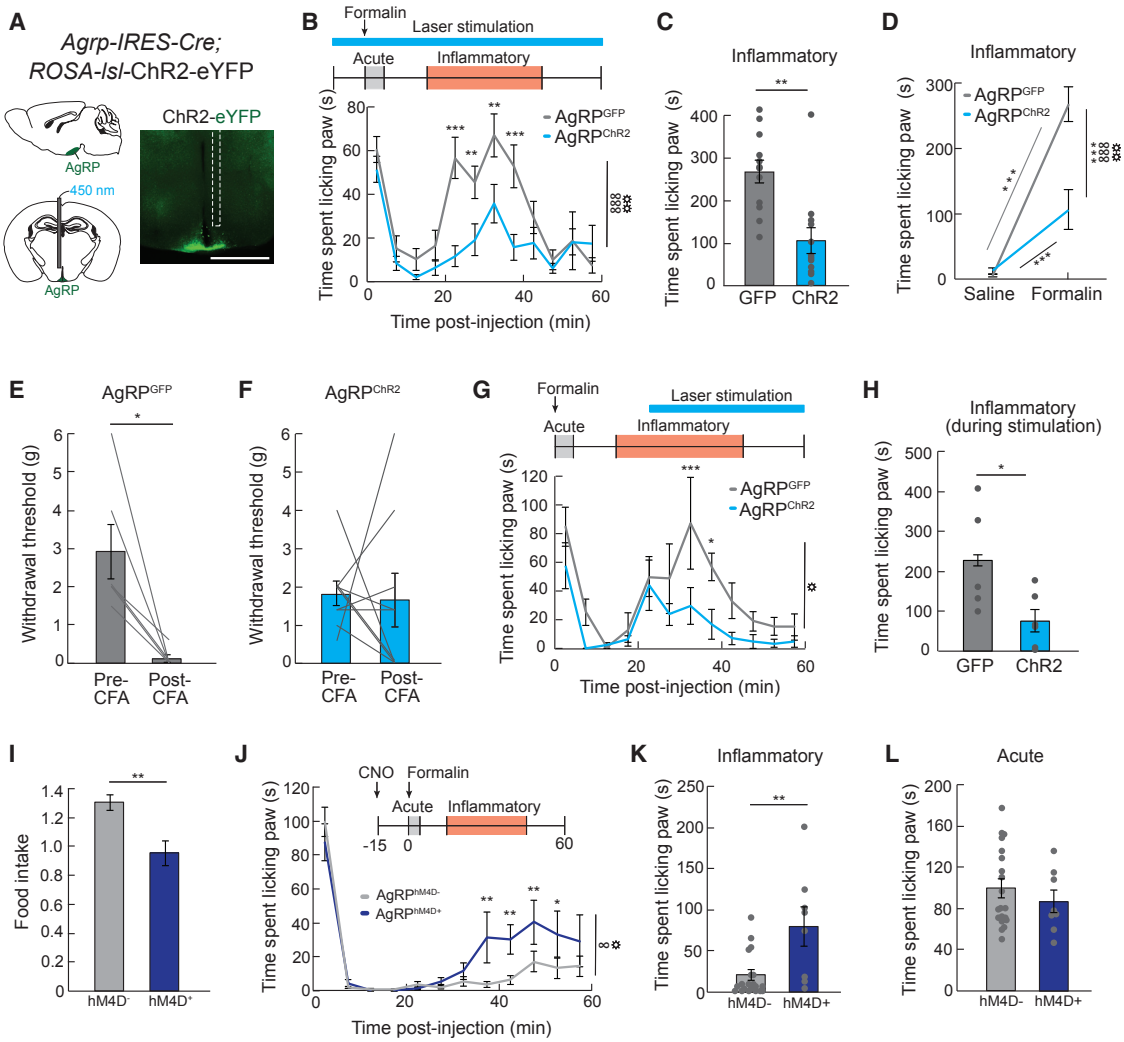

Figure 4. AgRP Neurons Mediate Suppression of Inflammatory Pain

(A) Schematic and representative image of ChR2 in *AgRP-IRES-Cre* mice implanted with an optical fiber (white dashed line indicates fiber track) above the ARC. Scale bar, 1 mm.

(B) Top, experimental design: 450 nm light pulse delivery began 10 min before formalin administration and continued for the duration of the formalin test. Bottom, graph: Time spent paw licking in $AgRP^{GFP}$ (n = 12) and $AgRP^{ChR2}$ (n = 12) mice following formalin administration (two-way repeated-measures ANOVA, $p < 0.001$).

(C) Inflammatory phase formalin-induced paw licking (time) in $AgRP^{GFP}$ and $AgRP^{ChR2}$ mice (unpaired t test, $p < 0.01$).

(D) Time spent licking paw during inflammatory phase following saline or formalin injection in $AgRP^{GFP}$ and $AgRP^{ChR2}$ mice (two-way repeated-measures ANOVA, $p < 0.001$).

(E) Withdrawal threshold (Von Frey filament at which mouse responded to >50% of trials) in $AgRP^{GFP}$ mice (n = 6) before and 24 hr post-CFA injection (paired t test, $p < 0.05$).

(F) Withdrawal threshold in $AgRP^{ChR2}$ mice (n = 9) before and 24 hr post-CFA injection (paired t test, p = ns).

(G) Top, experimental design: 450 nm light pulses were delivered beginning 25 min post-formalin injection and lasting through the duration of the session. Bottom, graph: time spent paw licking in $AgRP^{GFP}$ (n = 6) and $AgRP^{ChR2}$ (n = 6) mice (two-way repeated-measures ANOVA, main effect of stimulation [$AgRP^{GFP}$ versus $AgRP^{ChR2}$], $p < 0.05$).

(H) Inflammatory phase formalin-induced paw licking (time) during laser stimulation (25–45 min) in $AgRP^{GFP}$ and $AgRP^{ChR2}$ mice (unpaired t test, $p < 0.05$).

(I) Food intake in food-deprived $AgRP^{hM4D-}$ (n = 9) and $AgRP^{hM4D+}$ (n = 4) mice 4 hr following CNO injection (unpaired t test, $p < 0.01$).

(J) Time spent paw licking in $AgRP^{hM4D\geq}$ (n = 20) and $AgRP^{hM4D+}$ (n = 8) mice following formalin injection (two-way repeated-measures ANOVA, $p < 0.05$).

(K) Inflammatory phase formalin-induced paw licking (time) in $AgRP^{hM4D-}$ and $AgRP^{hM4D+}$ mice (unpaired t test, $p < 0.01$).

(L) Acute phase formalin-induced paw licking (time) in $AgRP^{hM4D-}$ and $AgRP^{hM4D+}$ mice (unpaired t test, p = ns). Data are expressed as mean ± SEM, ns $p > 0.05$, t tests and post hoc comparisons: *$p < 0.05$, **$p < 0.01$, ***$p < 0.001$; ANOVA interaction: ∞$p < 0.05$, ∞∞∞$p < 0.001$; ANOVA main effect of group: ☼$p < 0.05$, ☼☼$p < 0.01$.

See also Figures S2 and S3 and Table S1.

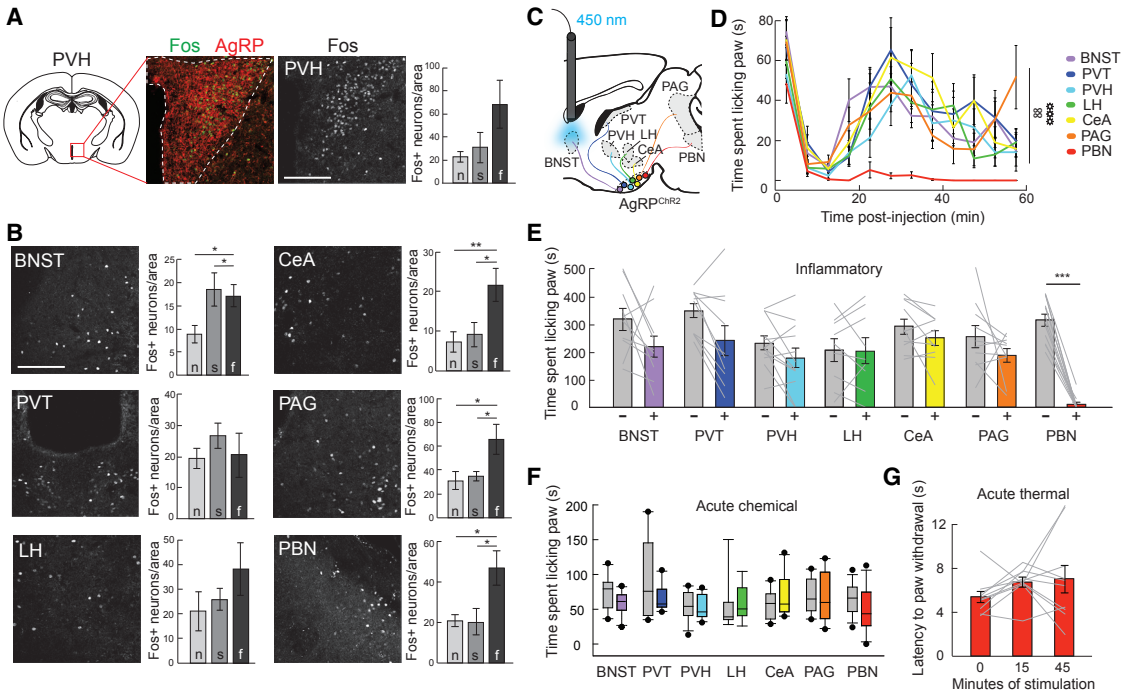

Figure 5. AgRP → PBN Neuron Activity Suppresses Inflammatory Pain

(A) Immediate early gene protein expression analysis was performed to detect changes in neural activity in AgRP neuron target regions following formalin paw injection. Fos$^+$ neurons in each target region (PVH depicted here) were quantified per unilateral brain section under the area of dense AgRP axonal projections (red, outlined by white dashed line). Scale bar, 150 μm. Graph depicts quantification of Fos$^+$ neurons in the PVH under AgRP axons following no treatment (n), saline paw injection (s), or formalin paw injection (f).

(B) Representative images and graphs depicting quantification of Fos$^+$ neurons under AgRP axons following no treatment (n), saline paw injection (s), or formalin paw injection (f) (n = 9, 2–4 images per mouse per target region, one-way ANOVA within brain region, $p < 0.05$ for BNST, CeA, PAG, PBN). Scale bar, 150 μm.

(C) Diagram of the major AgRP neuron projection subpopulations analyzed. Delivery of light to individual axon target fields of AgRP neurons (BNST shown here) allows for selective activation of discrete AgRP neuron projection subpopulations.

(D) Time spent paw licking following formalin injection during optogenetic stimulation of AgRP neuron projection subpopulations (n = 9–12/target region, two-way repeated-measures ANOVA, $p < 0.01$).

(E) Inflammatory phase formalin-induced paw licking (time) with (+, colored boxes) and without (−, gray boxes) AgRP neuron stimulation of discrete projection subpopulations (paired t tests with Bonferroni correction, all p values = ns except for PBN, $p < 0.001$).

(F) Acute phase formalin-induced paw licking (time) with (colored boxes) and without (gray boxes) AgRP neuron stimulation of discrete projection subpopulations (paired t tests with Bonferroni correction, all p values = ns).

(G) Latency to paw withdrawal from 52°C hotplate in AgRP → PBN^{ChR2} mice (n = 12, one-way ANOVA, p = ns). Data are expressed as mean ± SEM, ns $p > 0.05$, t tests and post hoc comparisons: *$p < 0.05$, **$p < 0.01$, ***$p < 0.001$; ANOVA interaction: ∞ ∞ $p < 0.01$; ANOVA main effect of group: ☼☼☼ $p < 0.001$.

See also Table S1.

activity (Figures S3G and S3H). Activating AgRP neurons that project to the CeA or the PAG had no effect on acute or inflammatory phase pain (Figures 5D–5F) nor did the delivery of light to AgRP^{GFP} → PBN mice (Figures S3I–S3K). This striking specificity of AgRP → PBN neuron function demonstrates that the PBN is a neural substrate for the interaction between hunger and inflammatory pain.

NPY Signaling in the Lateral PBN Inhibits Inflammatory Pain

To explore how AgRP → PBN signaling intersects with the neural representation of inflammatory pain, we first examined the anatomical overlap of AgRP projections and neurons activated by inflammatory pain. We find a dense AgRP axonal projection in the lateral PBN (lPBN) and a more medial projection to the locus coeruleus area (Figure 6A). AgRP axons projecting to the lPBN overlap with neurons activated by formalin paw injection (Figure S4A), suggesting the activity in AgRP neurons projecting to the lPBN mediates inflammatory pain.

Because AgRP neuron activity is both necessary and sufficient to provide a protective effect against inflammatory pain during hunger (Figure 4), we next sought to determine the molecular signals in the PBN that mediate the suppression of pain during hunger. We first explored protein expression of the 3 main neurotransmitters of AgRP neurons: NPY, GABA, and AgRP. Expression of both NPY and the GABA synthetic enzyme GAD65 were increased in axon terminals of AgRP → lPBN neurons during hunger (Figures 6B and 6C), suggesting these molecules may mediate the interaction between hunger and pain in the lPBN. To test the functional relevance of these neurotransmitters, we performed microinjections of each neurotransmitter into the lPBN immediately before formalin paw injection. NPY

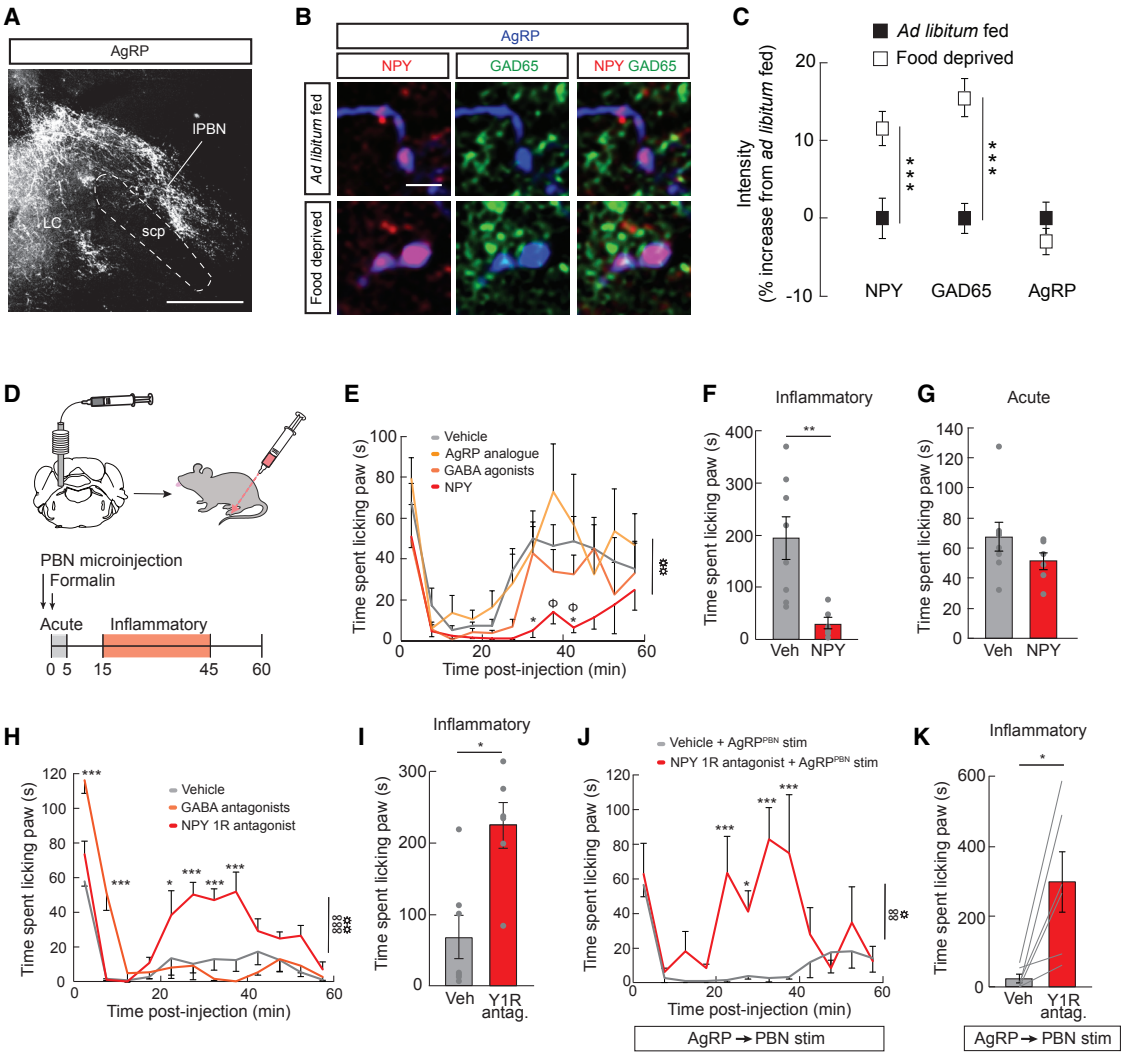

Figure 6. Lateral PBN NPY Signaling Suppresses Inflammatory Pain

(A) Representative image of AgRP fibers terminating in the lateral PBN (lPBN) and locus coeruleus area. LC, locus coeruleus; lPBN, lateral PBN; scp, superior cerebellar peduncle. Scale bar, 500 μm.

(B) Representative images of NPY (red), GAD65 (green), and AgRP (blue) immunofluorescence in AgRP → lPBN neuron boutons of *ad libitum*-fed and 24-hr food-deprived mice. Scale bar, 5 μm.

(C) Average intensity of NPY, GAD65, and AgRP immunofluorescence in 24-hr food-deprived mice (n = 3 mice, 256 boutons) relative to *ad libitum*-fed controls (n = 2 mice, 366 boutons) (unpaired t tests, $p < 0.001$).

(D) Experimental design: lPBN microinjections were performed immediately before formalin paw injection.

(E) Formalin-induced paw licking (time) in lPBN vehicle-, NPY-, GABA agonists-, and AgRP analog-microinjected mice (n = 6–8/group, two-way ANOVA, main effect of drug $p < 0.01$). Post hoc comparisons: *$p < 0.05$ vehicle versus NPY; Φ$p < 0.05$ NPY versus AgRP analog.

(F) Inflammatory phase formalin-induced paw licking (time) in lPBN vehicle- and NPY-microinjected mice (unpaired t test, $p < 0.01$).

(G) Acute phase formalin-induced paw licking (time) in lPBN vehicle- and NPY-microinjected mice (unpaired t test, p = ns).

(H) Formalin-induced paw licking (time) in lPBN vehicle-, Y1 receptor (Y1R) antagonist-, and GABA receptor antagonist-microinjected mice (n = 6–7/group, two-way repeated-measures ANOVA, $p < 0.001$).

(I) Inflammatory phase formalin-induced paw licking (time) in lPBN vehicle- and Y1R antagonist-microinjected mice (unpaired t test, $p < 0.05$).

(J) Formalin-induced paw licking (time) in lPBN vehicle- and Y1 receptor (Y1R) antagonist-microinjected mice with AgRP → PBN neuron stimulation (n = 6, two-way repeated-measures ANOVA, $p < 0.01$).

(K) Inflammatory phase formalin-induced paw licking (time) in lPBN vehicle- and Y1R antagonist-microinjected mice with AgRP → PBN neuron stimulation (unpaired t test, $p < 0.05$). Data are expressed as mean ± SEM, ns $p > 0.05$, t tests and post hoc comparisons: *$p < 0.05$, **$p < 0.01$, ***$p < 0.001$; ANOVA interaction: ∞∞$p < 0.01$, ∞∞∞$p < 0.001$; ANOVA main effect of drug: ☼$p < 0.05$, ☼☼$p < 0.01$, ☼☼☼$p < 0.001$.

Figures S4 and S5 and Table S1.

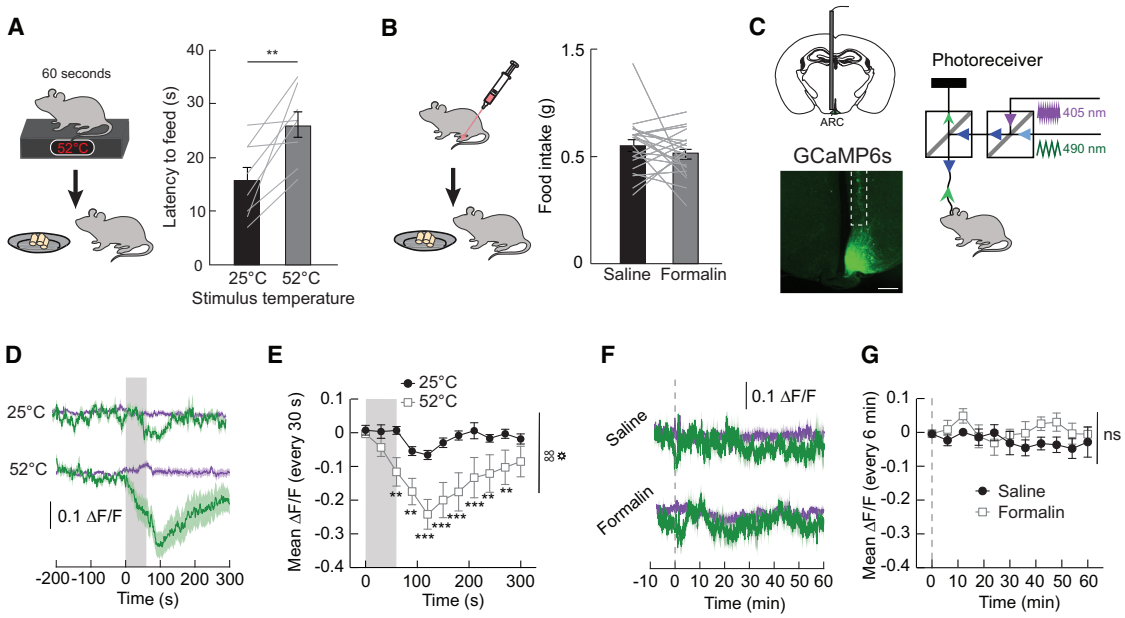

Figure 7. Acute Pain Inhibits Feeding Behavior and Activity in AgRP Neurons

(A) Left, experimental design: latency to feed (first bite) was measured following 60 s exposure to a 52°C hotplate. Right, graph: latency to feed after 60 s exposure to either a 25°C or 52°C plate (n = 8, paired t test, $p < 0.01$).

(B) Left, experimental design: 1-hr food intake was measured after formalin paw injection. Right, graph: 1-hr food intake in food-deprived mice after paw injection of saline or formalin (n = 21, paired t test, p = ns).

(C) Left: schematic and representative image of expression of the calcium indicator GCaMP6s in AgRP neurons. Scale bar, 500 μm. Right: configuration for monitoring calcium dynamics *in vivo* using GCaMP6s expressed in AgRP neurons. The 490 nm excitation activates the calcium-dependent GCaMP6s signal and the 405 nm excitation activates the calcium-independent (*isosbestic*) GCaMP6s fluorescence.

(D) Calcium-dependent (mean, dark green; SEM, green shading) and calcium-independent (mean, dark purple; SEM, purple shading) change in fluorescence (ΔF/F) in AgRP neurons following exposure to 25°C or 52°C plate (n = 10). Grey-shaded region indicates time exposed to hotplate.

(E) Quantification of change in fluorescence (30-s time bins) in mice following exposure to 25°C or 52°C plate (n = 10, two-way repeated-measures ANOVA, $p < 0.01$).

(F) Calcium-dependent (mean, dark green; SEM, green shading) and calcium-independent (mean, dark purple; SEM, purple shading) change in fluorescence (ΔF/F) in AgRP neurons following saline or formalin paw injection (n = 8). Dashed line indicates time of paw injection.

(G) Quantification of change in fluorescence (6-min time bins) in mice following saline or formalin paw injection (n = 8, two-way repeated-measures ANOVA, p = ns). Data are expressed as mean ± SEM, ns $p > 0.05$, t tests and post hoc comparisons: **$p < 0.01$, ***$p < 0.001$; ANOVA interaction: ∞ ∞ $p < 0.01$; ANOVA main effect of group: ☼$p < 0.05$.

See also Figure S6 and Table S1.

signaling in the lPBN robustly and selectively attenuated inflammatory phase pain responses, without affecting acute pain responses or food intake (Figures 6D–6G and S4B). Conversely, neither GABA nor AgRP signaling in the lPBN (Figure 6E), nor NPY in the locus coeruleus area (Figures S4C–S4F), had any effect on formalin-induced pain responses. Consistent with the kinetics of NPY signaling on behavior (Stanley and Leibowitz, 1985), the onset (Figures S4G and S4I) and offset (Figures S4H and S4I) of AgRP → PBN neuron activity during an ongoing inflammatory phase pain response triggered changes in nocifensive behavior within minutes.

To determine if NPY signaling in the lPBN functions in a physiologically relevant manner, we next assessed the role of endogenous NPY signaling during hunger. Strikingly, blocking NPY Y1 receptors (Atasoy et al., 2012) in the lPBN of food-deprived mice reversed the analgesic effects of hunger (Figures 6H and 6I) while antagonism of GABA receptors did not affect inflammatory pain (Figure 6H). Furthermore, blockade of Y1 receptors in the lPBN attenuated the suppression of inflammatory pain by AgRP → PBN neuron stimulation (Figure 6J and 6K), suggesting that AgRP neurons are the source of the analgesic NPY. This reduction in pain is likely mediated by glutamatergic neurons in the lPBN as inhibiting VGlut2-expressing, but not Gad2-expressing, neurons in the lPBN during the formalin assay reduced inflammatory pain (Figure S5). Taken together, these data demonstrate that lPBN NPY signaling is both necessary and sufficient for the suppression of inflammatory pain.

Acute Pain Reduces Food Seeking and Neural Activity in Hunger Circuits

Survival requires ranking and responding to the most critical need at a given time. Because hunger does not suppress the response to acute pain, we reasoned that neural mechanisms may exist to deprioritize hunger during threats to survival such as acute pain. Exposure to a 52°C hotplate increased the latency to feed in 24-hr food-deprived mice (Figure 7A). However, no change in food intake in hungry mice during inflammatory pain was observed (Figure 7B). To gain insight into the mechanisms

through which acute pain inhibits feeding behavior, we next measured *in vivo* calcium dynamics in AgRP neurons as a proxy for neural activity (Figure 7C) (Gunaydin et al., 2014). Chow presentation significantly reduced the activity of AgRP neurons in hungry mice (Figure S6A and S6B), as previously reported (Betley et al., 2015; Chen et al., 2015; Mandelblat-Cerf et al., 2015). Consistent with the effects of pain on food intake, acute thermal pain, but not formalin injection, reduced the activity of AgRP neurons (Figures 7D–7G, Figure S6C and S6D). This suppression of AgRP neuron activity by acute thermal pain reached a magnitude comparable to ~50% of the suppression observed upon refeeding hungry mice (Figure S6E). Together, these data suggest that acute thermal pain can influence behavior by suppressing activity in AgRP neuron circuits.

DISCUSSION

Here, we discovered a bidirectional interaction between hunger and pain and revealed a neural mechanism that processes competing survival signals. We demonstrated that hunger selectively attenuates the behavioral and affective responses to inflammatory pain. This effect is centrally mediated by a small subset of AgRP neurons that project to the PBN. The suppression of inflammatory pain by hunger requires NPY signaling through Y1 receptors. Conversely, acute but not inflammatory pain inhibited feeding behavior and reduced the endogenous activity of AgRP neurons during hunger. These findings demonstrate the utility of examining intersecting survival needs to reveal neural circuits that influence behavior, as we have identified a mechanism for the inhibition of inflammatory pain.

Bidirectional Behavioral Interaction between Hunger and Pain

It has been demonstrated that hunger can both increase and decrease responses to pain (Bodnar et al., 1978a; Hamm and Lyeth, 1984; Hargraves and Hentall, 2005; LaGraize et al., 2004; Pollatos et al., 2012), suggesting that these two broadly tuned survival signals may interact in a hierarchical manner. We found that 24-hr food deprivation consistently and dramatically attenuates responses to inflammatory pain, but has no effect on thermal pain, mechanical pain, or the acute response to formalin paw injection. In comparison to previous studies, we observed two striking results. First, hunger had no effect on acute pain resulting from thermal, mechanical, or chemical insult. While previous reports demonstrate that hunger modestly reduces (10%–20%) acute pain (Bodnar et al., 1978a; Hamm and Lyeth, 1984; Hargraves and Hentall, 2005), the majority of the acute pain responses are left intact—an important ethological consideration to enhance survival. Second, we found that hunger selectively and almost completely abolished inflammatory pain responses, mimicking the effects of anti-inflammatory painkillers. This profound suppression, even without the distractor of food, suggests an analgesic effect of hunger and provides a behavioral mechanism to facilitate food seeking following an injury. Taken together, our observations demonstrate that hunger has the ability to selectively inhibit long-term pain responses while leaving intact the adaptive ability to respond to acutely painful stimuli.

The robust suppression of inflammatory pain response by food deprivation prompted us to explore how hunger affects other dimensions of pain. Pain induces negative emotional responses, and it is thought that distinct neural systems regulate the sensory and affective components of pain (Johansen and Fields, 2004). Given that hunger is a complex motivational state that involves coordination of many distinct neural circuits (Andermann and Lowell, 2017; Grill, 2006), it is not surprising that hunger can interface with both the sensory and affective components of pain. Indeed, the affective components of pain were diminished by hunger, as hunger attenuated a place avoidance of cues previously associated with inflammatory pain. The ability of hunger to inhibit both the unpleasant aspects of pain in addition to behavioral responses to pain suggests an analgesic effect of hunger. These findings have implications not only for the treatment of pain disorders but also for the treatment of affective disorders such as depression that are highly comorbid with conditions of chronic pain (Miller and Cano, 2009; Price, 2000).

Hunger attenuated inflammatory but not acute pain, but only acute pain was capable of inhibiting feeding behavior. Furthermore, acute thermal pain directly inhibited the activity of hunger-sensitive AgRP neurons, suggesting that pain is not simply a distractor from hunger. The transient reduction in AgRP neuron activity is consistent with our observation of short- but not long-term reductions in feeding behavior following painful stimuli. While other studies have reported robust reductions in endogenous AgRP neuron activity by food (Betley et al., 2015; Chen et al., 2015; Mandelblat-Cerf et al., 2015), our findings unexpectedly provide a feeding-independent mechanism that inhibits this neural population.

Together, our data show that acute pain inhibits hunger, and that hunger inhibits inflammatory pain. This hierarchical interaction between hunger and different modalities of pain suggests a prioritization of survival needs, whereby behavior addresses the most urgent environmental or physiological stimulus. Together, these observations are ethologically sound for survival, as they describe a system that reliably responds to acute threat but allows for the suppression of longer-term pain when food seeking behavior is paramount for survival.

Neural and Molecular Mechanisms for the Inhibition of Pain

Activation of AgRP neurons suppressed inflammatory pain, revealing a common neural substrate for circuits that mediate hunger and pain. It is well established that AgRP neuron signaling influences complex behaviors that promote food seeking (Burnett et al., 2016; Dietrich et al., 2015; Krashes et al., 2011; Padilla et al., 2016). The ability of AgRP neuron activity to robustly inhibit inflammatory pain was surprising because analgesia is not an obvious priority for food seeking. However, facilitating feeding behavior following injury likely requires hard-wired neural circuitry to overcome obstacles such as pain. Interestingly, the AgRP neural network, which is composed of parallel projections that do not all drive food intake (Betley et al., 2013), provides an anatomical arrangement that allows distinct projections to inhibit neural processing of environmental signals that impede feeding.

To unravel the AgRP circuitry that inhibits inflammatory pain, we performed a systematic functional assessment of AgRP neuron subpopulations that revealed the striking specificity by which a tiny population of neurons can initiate behavioral switching. Indeed, activity in only ~300 AgRP neurons that project to the PBN (Betley et al., 2013) specifically eliminated inflammatory pain. The magnitude of suppression of inflammatory pain was comparable to morphine and was more robust than most anti-inflammatory or steroid analgesics (Hunskaar and Hole, 1987). Given that activity in AgRP → PBN neurons is insufficient to drive food intake, the suppression of pain is not simply a consequence of being distracted by an ongoing hunger state. Rather, these neurons facilitate food seeking by reducing responses to competing aversive drives or stimuli that are processed in the PBN (Carter et al., 2013). Furthermore, this function of a feeding insufficient subpopulation highlights the importance of the distributed AgRP neuron circuitry—as this population of hunger-sensitive neurons has distinct subpopulations that interact with many systems in the brain to regulate other survival behaviors.

Manipulating AgRP → PBN neurons during an ongoing pain response causes changes in nocifensive behavior within minutes. This result suggests that peptidergic neurotransmission mediates the interaction between hunger and pain. Indeed, NPY signaling inhibited the behavioral response to inflammatory pain. We corroborated these data by showing that Y1R antagonism in the PBN selectively blocked the ability of hunger or AgRP → PBN stimulation to attenuate inflammatory pain. This occlusion of the dominant NPY receptor in the PBN (Alhadeff et al., 2015) demonstrates the necessity and sufficiency of NPY Y1 receptor signaling for the inhibition of inflammatory pain. Genetic (Naveilhan et al., 2001) and pharmacological (Solway et al., 2011) evidence demonstrate a role of NPY Y1 receptor in the dorsal horn of the spinal cord in mediating pain. Within the brain, it has been demonstrated that NPY signaling in the PAG and trigeminal nucleus also inhibits pain (Martins-Oliveira et al., 2016; Wang et al., 2001). Here, our findings uncover the PBN as an additional site of action for the analgesic effects of NPY and are unique in that they selectively inhibit inflammatory pain.

GABA and AgRP signaling in the PBN have documented roles in energy balance control (Higgs and Cooper, 1996; Skibicka and Grill, 2009). Furthermore, GABA signaling from AgRP neurons projecting to the PBN is permissive for feeding (Wu et al., 2009), as it suppresses the visceral malaise associated with consumption of a large meal or toxic substance (Alhadeff et al., 2017; Campos et al., 2016; Carter et al., 2013; Essner et al., 2017). However, GABA and AgRP agonists microinjected into the PBN did not affect acute or inflammatory pain, highlighting NPY as the molecular meditator of pain in the PBN. While co-release of neurotransmitters is well-documented (Hnasko et al., 2010; Jonas et al., 1998), our findings dissociate distinct behavioral functions for co-transmitters released by a single neuron type.

Both hunger and pain are negative signals that individuals try to avoid (Betley et al., 2015; Johansen and Fields, 2004; Keys, 1946). The finding that hunger inhibits inflammatory pain raises the question of how one negative drive can inhibit another. Our neural circuit analysis provides insight into this paradox. Because AgRP → PBN neuron activity does not evoke food intake (Atasoy et al., 2012), it is unlikely that these neurons mediate the negative valence of hunger (Betley et al., 2015). Our findings conclusively implicate AgRP → PBN signaling in mediating the response to pain. However, the distinct AgRP circuits that mediate the negative valence of hunger, and inhibit the negative valence of pain, remain compelling topics for future investigation.

Conclusion

Our findings uncover a hierarchy of survival behaviors that prioritizes needs in a changing environment. Our behavioral observations provided a unique entry point to study circuits that inhibit pain. This unexpected ability to influence pain through activity in a distinct hypothalamic → hindbrain hunger circuit reveals an endogenous and ethologically relevant neural circuit mechanism for analgesia. Importantly, this neural circuit can be manipulated to inhibit potentially maladaptive inflammatory pain without compromising adaptive responses to painful stimuli that may acutely threaten survival. Through developing a mechanistic understanding of the influence of hunger on nociception, these experiments provide novel targets for the development of pain management therapies, which is of utmost importance in the search for non-addictive analgesics.

STAR★METHODS

Detailed methods are provided in the online version of this paper and include the following:

- KEY RESOURCES TABLE
- CONTACT FOR REAGENT AND RESOURCE SHARING
- EXPERIMENTAL MODEL AND SUBJECT DETAILS
- METHOD DETAILS
  - Recombinant Adeno-Associated Virus (rAAV) Constructs and Production:
  - Viral Injections, Fiber Optic and Cannula Placement:
  - General Experimental Design:
  - In Vivo Photostimulation:
  - Food Deprivation/Restriction:
  - Inflammatory Pain Measurements (Formalin Test):
  - Thermal Pain Measurements (Hotplate Test):
  - Mechanical Pain Measurements (Von Frey Test):
  - Inflammation-Induced Sensitization:
  - Conditioned Place Avoidance:
  - Immunohistochemistry and Imaging:
  - Pharmacology:
  - Fiber Photometry:
- QUANTIFICATION AND STATISTICAL ANALYSIS

SUPPLEMENTAL INFORMATION

Supplemental Information includes six figures and three tables and can be found with this article online at https://doi.org/10.1016/j.cell.2018.02.057.

ACKNOWLEDGMENTS

We thank S. Pulido, B. Jannuzi, O. Park, C. Shin, K. Patel, I. Cogdell, R. Ly, O. Green, and P. Ehmann for experimental assistance and S. Sternson, H. Grill,

M. Schmidt, and A. Chen for comments on the manuscript. This research was funded by the University of Pennsylvania School of Arts and Sciences (to J.N.B.), the American Heart Association (AHA) (17SDG33400158 to J.N.B.), the Whitehall Foundation (to J.N.B), and the NIH (1R01DK114104 to J.N.B, 2T32DK7314-36 and F32DK112561-01 to A.L.A., and R01DK114812 to B.C.D.J.).

AUTHOR CONTRIBUTIONS

A.L.A. and J.N.B. initiated the project and prepared the manuscript with comments from all authors. A.L.A., Z.S., E.H., M.L.K., R.A.H., B.C.D.J., and J.N.B. designed experiments and analyzed data. C.G. and A.W.H. developed FlpO mice. A.L.A., Z.S., E.H., M.L.K., S.Z.P., R.A.H., and J.N.B. performed experiments.

DECLARATION OF INTERESTS

The authors declare no competing interests.

Received: August 18, 2017
Revised: December 4, 2017
Accepted: February 21, 2018
Published: March 22, 2018

REFERENCES

Alhadeff, A.L., Golub, D., Hayes, M.R., and Grill, H.J. (2015). Peptide YY signaling in the lateral parabrachial nucleus increases food intake through the Y1 receptor. Am. J. Physiol. Endocrinol. Metab. *309*, E759–E766.

Alhadeff, A.L., Holland, R.A., Zheng, H., Rinaman, L., Grill, H.J., and De Jonghe, B.C. (2017). Excitatory hindbrain-forebrain communication is required for cisplatin-induced anorexia and weight loss. J. Neurosci. *37*, 362–370.

Andermann, M.L., and Lowell, B.B. (2017). Toward a wiring diagram understanding of appetite control. Neuron *95*, 757–778.

Aponte, Y., Atasoy, D., and Sternson, S.M. (2011). AGRP neurons are sufficient to orchestrate feeding behavior rapidly and without training. Nat. Neurosci. *14*, 351–355.

Atasoy, D., Betley, J.N., Su, H.H., and Sternson, S.M. (2012). Deconstruction of a neural circuit for hunger. Nature *488*, 172–177.

Baulmann, J., Spitznagel, H., Herdegen, T., Unger, T., and Culman, J. (2000). Tachykinin receptor inhibition and c-Fos expression in the rat brain following formalin-induced pain. Neuroscience *95*, 813–820.

Betley, J.N., Wright, C.V., Kawaguchi, Y., Erdélyi, F., Szabó, G., Jessell, T.M., and Kaltschmidt, J.A. (2009). Stringent specificity in the construction of a GABAergic presynaptic inhibitory circuit. Cell *139*, 161–174.

Betley, J.N., Cao, Z.F., Ritola, K.D., and Sternson, S.M. (2013). Parallel, redundant circuit organization for homeostatic control of feeding behavior. Cell *155*, 1337–1350.

Betley, J.N., Xu, S., Cao, Z.F.H., Gong, R., Magnus, C.J., Yu, Y., and Sternson, S.M. (2015). Neurons for hunger and thirst transmit a negative-valence teaching signal. Nature *521*, 180–185.

Bodnar, R.J., Kelly, D.D., Spiaggia, A., and Glusman, M. (1977). Analgesia Produced by Cold-Water Stress - Effect of Naloxone. Fed. Proc. *36*, 1010–1010.

Bodnar, R.J., Kelly, D.D., Spiaggia, A., and Glusman, M. (1978a). Biphasic alterations of nociceptive thresholds induced by food-deprivation. Physiol. Psychol. *6*, 391–395.

Bodnar, R.J., Kelly, D.D., Steiner, S.S., and Glusman, M. (1978b). Stress-produced analgesia and morphine-produced analgesia: lack of cross-tolerance. Pharmacol. Biochem. Behav. *8*, 661–666.

Burnett, C.J., Li, C., Webber, E., Tsaousidou, E., Xue, S.Y., Brüning, J.C., and Krashes, M.J. (2016). Hunger-driven motivational state competition. Neuron *92*, 187–201.

Campos, C.A., Bowen, A.J., Schwartz, M.W., and Palmiter, R.D. (2016). Parabrachial CGRP Neurons Control Meal Termination. Cell Metab. *23*, 811–820.

Carey, L.M., Gutierrez, T., Deng, L., Lee, W.H., Mackie, K., and Hohmann, A.G. (2017). Inflammatory and Neuropathic Nociception is Preserved in GPR55 Knockout Mice. Sci. Rep. *7*, 944.

Carter, M.E., Soden, M.E., Zweifel, L.S., and Palmiter, R.D. (2013). Genetic identification of a neural circuit that suppresses appetite. Nature *503*, 111–114.

Chen, Y., Lin, Y.C., Kuo, T.W., and Knight, Z.A. (2015). Sensory detection of food rapidly modulates arcuate feeding circuits. Cell *160*, 829–841.

Coderre, T.J., Vaccarino, A.L., and Melzack, R. (1990). Central nervous system plasticity in the tonic pain response to subcutaneous formalin injection. Brain Res. *535*, 155–158.

Deyama, S., Yamamoto, J., Machida, T., Tanimoto, S., Nakagawa, T., Kaneko, S., Satoh, M., and Minami, M. (2007). Inhibition of glutamatergic transmission by morphine in the basolateral amygdaloid nucleus reduces pain-induced aversion. Neurosci. Res. *59*, 199–204.

Dietrich, M.O., Zimmer, M.R., Bober, J., and Horvath, T.L. (2015). Hypothalamic Agrp neurons drive stereotypic behaviors beyond feeding. Cell *160*, 1222–1232.

Dubuisson, D., and Dennis, S.G. (1977). The formalin test: a quantitative study of the analgesic effects of morphine, meperidine, and brain stem stimulation in rats and cats. Pain *4*, 161–174.

Essner, R.A., Smith, A.G., Jamnik, A.A., Ryba, A.R., Trutner, Z.D., and Carter, M.E. (2017). AgRP neurons can increase food intake during conditions of appetite suppression and inhibit anorexigenic parabrachial neurons. J. Neurosci. *37*, 8678–8687.

Grill, H.J. (2006). Distributed neural control of energy balance: contributions from hindbrain and hypothalamus. Obesity (Silver Spring) *14* (*Suppl 5*), 216S–221S.

Gunaydin, L.A., Grosenick, L., Finkelstein, J.C., Kauvar, I.V., Fenno, L.E., Adhikari, A., Lammel, S., Mirzabekov, J.J., Airan, R.D., Zalocusky, K.A., et al. (2014). Natural neural projection dynamics underlying social behavior. Cell *157*, 1535–1551.

Hamm, R.J., and Lyeth, B.G. (1984). Nociceptive thresholds following food restriction and return to free-feeding. Physiol. Behav. *33*, 499–501.

Hargraves, W.A., and Hentall, I.D. (2005). Analgesic effects of dietary caloric restriction in adult mice. Pain *114*, 455–461.

Higgs, S., and Cooper, S.J. (1996). Hyperphagia induced by direct administration of midazolam into the parabrachial nucleus of the rat. Eur. J. Pharmacol. *313*, 1–9.

Hnasko, T.S., Chuhma, N., Zhang, H., Goh, G.Y., Sulzer, D., Palmiter, R.D., Rayport, S., and Edwards, R.H. (2010). Vesicular glutamate transport promotes dopamine storage and glutamate corelease in vivo. Neuron *65*, 643–656.

Hunskaar, S., and Hole, K. (1987). The formalin test in mice: dissociation between inflammatory and non-inflammatory pain. Pain *30*, 103–114.

Jikomes, N., Ramesh, R.N., Mandelblat-Cerf, Y., and Andermann, M.L. (2016). Preemptive stimulation of AgRP neurons in fed mice enables conditioned food seeking under threat. Curr. Biol. *26*, 2500–2507.

Johansen, J.P., and Fields, H.L. (2004). Glutamatergic activation of anterior cingulate cortex produces an aversive teaching signal. Nat. Neurosci. *7*, 398–403.

Jonas, P., Bischofberger, J., and Sandkühler, J. (1998). Corelease of two fast neurotransmitters at a central synapse. Science *281*, 419–424.

Keys, A. (1946). Experimental human starvation; general and metabolic results of a loss of one fourth the body weight in six months. Fed. Proc. *5*, 55.

Krashes, M.J., Koda, S., Ye, C., Rogan, S.C., Adams, A.C., Cusher, D.S., Maratos-Flier, E., Roth, B.L., and Lowell, B.B. (2011). Rapid, reversible activation of AgRP neurons drives feeding behavior in mice. J. Clin. Invest. *121*, 1424–1428.

LaGraize, S.C., Borzan, J., Rinker, M.M., Kopp, J.L., and Fuchs, P.N. (2004). Behavioral evidence for competing motivational drives of nociception and hunger. Neurosci. Lett. *372*, 30–34.

Lein, E.S., Hawrylycz, M.J., Ao, N., Ayres, M., Bensinger, A., Bernard, A., Boe, A.F., Boguski, M.S., Brockway, K.S., Byrnes, E.J., et al. (2007). Genome-wide atlas of gene expression in the adult mouse brain. Nature *445*, 168–176.

Lerner, T.N., Shilyansky, C., Davidson, T.J., Evans, K.E., Beier, K.T., Zalocusky, K.A., Crow, A.K., Malenka, R.C., Luo, L., Tomer, R., and Deisseroth, K. (2015). Intact-brain analyses reveal distinct information carried by SNc dopamine subcircuits. Cell *162*, 635–647.

Li, H., Penzo, M.A., Taniguchi, H., Kopec, C.D., Huang, Z.J., and Li, B. (2013). Experience-dependent modification of a central amygdala fear circuit. Nat. Neurosci. *16*, 332–339.

Liu, P., Jenkins, N.A., and Copeland, N.G. (2003). A highly efficient recombineering-based method for generating conditional knockout mutations. Genome Res. *13*, 476–484.

Loeser, J.D. (2012). Relieving pain in America. Clin. J. Pain *28*, 185–186.

Luquet, S., Perez, F.A., Hnasko, T.S., and Palmiter, R.D. (2005). NPY/AgRP neurons are essential for feeding in adult mice but can be ablated in neonates. Science *310*, 683–685.

Madisen, L., Mao, T., Koch, H., Zhuo, J.M., Berenyi, A., Fujisawa, S., Hsu, Y.W., Garcia, A.J., 3rd, Gu, X., Zanella, S., et al. (2012). A toolbox of Cre-dependent optogenetic transgenic mice for light-induced activation and silencing. Nat. Neurosci. *15*, 793–802.

Mandelblat-Cerf, Y., Ramesh, R.N., Burgess, C.R., Patella, P., Yang, Z., Lowell, B.B., and Andermann, M.L. (2015). Arcuate hypothalamic AgRP and putative POMC neurons show opposite changes in spiking across multiple timescales. eLife *4*, e07122.

Marchand, F., Perretti, M., and McMahon, S.B. (2005). Role of the immune system in chronic pain. Nat. Rev. Neurosci. *6*, 521–532.

Martins-Oliveira, M., Akerman, S., Tavares, I., and Goadsby, P.J. (2016). Neuropeptide Y inhibits the trigeminovascular pathway through NPY Y1 receptor: implications for migraine. Pain *157*, 1666–1673.

Miller, L.R., and Cano, A. (2009). Comorbid chronic pain and depression: who is at risk? J. Pain *10*, 619–627.

Mu, D., Deng, J., Liu, K.F., Wu, Z.Y., Shi, Y.F., Guo, W.M., Mao, Q.Q., Liu, X.J., Li, H., and Sun, Y.G. (2017). A central neural circuit for itch sensation. Science *357*, 695–699.

Naveilhan, P., Hassani, H., Lucas, G., Blakeman, K.H., Hao, J.X., Xu, X.J., Wiesenfeld-Hallin, Z., Thorén, P., and Ernfors, P. (2001). Reduced antinociception and plasma extravasation in mice lacking a neuropeptide Y receptor. Nature *409*, 513–517.

Padilla, S.L., Qiu, J., Soden, M.E., Sanz, E., Nestor, C.C., Barker, F.D., Quintana, A., Zweifel, L.S., Rønnekleiv, O.K., Kelly, M.J., and Palmiter, R.D. (2016). Agouti-related peptide neural circuits mediate adaptive behaviors in the starved state. Nat. Neurosci. *19*, 734–741.

Pavlov, I.P., and Fol'bort, G.V. (1926). Die höchste Nerventätigkeit (das Verhalten) von Tieren. Eine zwanzigjährige Prüfung der objektiven Forschung ; Bedingte Reflexe. Sammlung von Artikeln, Berichten, Vorlesungen und Reden, 3. Aufl., übers. von G. Volbroth, ed. (München: J. F. Bergmann).

Penzo, M.A., Robert, V., Tucciarone, J., De Bundel, D., Wang, M., Van Aelst, L., Darvas, M., Parada, L.F., Palmiter, R.D., He, M., et al. (2015). The paraventricular thalamus controls a central amygdala fear circuit. Nature *519*, 455–459.

Pollatos, O., Herbert, B.M., Füstös, J., Weimer, K., Enck, P., and Zipfel, S. (2012). Food deprivation sensitizes pain perception. J. Psychophysiol. *26*, 1–9.

Price, D.D. (2000). Psychological and neural mechanisms of the affective dimension of pain. Science *288*, 1769–1772.

Skibicka, K.P., and Grill, H.J. (2009). Hypothalamic and hindbrain melanocortin receptors contribute to the feeding, thermogenic, and cardiovascular action of melanocortins. Endocrinology *150*, 5351–5361.

Solway, B., Bose, S.C., Corder, G., Donahue, R.R., and Taylor, B.K. (2011). Tonic inhibition of chronic pain by neuropeptide Y. Proc. Natl. Acad. Sci. USA *108*, 7224–7229.

Stanley, B.G., and Leibowitz, S.F. (1985). Neuropeptide Y injected in the paraventricular hypothalamus: a powerful stimulant of feeding behavior. Proc. Natl. Acad. Sci. USA *82*, 3940–3943.

Sternson, S.M., and Eiselt, A.K. (2017). Three Pillars for the Neural Control of Appetite. Annu. Rev. Physiol. *79*, 401–423.

Su, Z., Alhadeff, A.L., and Betley, J.N. (2017). Nutritive, Post-ingestive Signals Are the Primary Regulators of AgRP Neuron Activity. Cell Rep. *21*, 2724–2736.

Tinbergen, N. (1951). The Study of Instinct (Oxford University Press).

Tong, Q., Ye, C.P., Jones, J.E., Elmquist, J.K., and Lowell, B.B. (2008). Synaptic release of GABA by AgRP neurons is required for normal regulation of energy balance. Nat. Neurosci. *11*, 998–1000.

Wang, J.Z., Lundeberg, T., and Yu, L.C. (2001). Anti-nociceptive effect of neuropeptide Y in periaqueductal grey in rats with inflammation. Brain Res. *893*, 264–267.

Wu, Q., Boyle, M.P., and Palmiter, R.D. (2009). Loss of GABAergic signaling by AgRP neurons to the parabrachial nucleus leads to starvation. Cell *137*, 1225–1234.

Zhu, H., Aryal, D.K., Olsen, R.H., Urban, D.J., Swearingen, A., Forbes, S., Roth, B.L., and Hochgeschwender, U. (2016). Cre-dependent DREADD (Designer Receptors Exclusively Activated by Designer Drugs) mice. Genesis *54*, 439–446.

STAR★METHODS

KEY RESOURCES TABLE

REAGENT or RESOURCE	SOURCE	IDENTIFIER
Antibodies		
Goat anti-AgRP	Neuromics	GT15023
Rabbit anti-cFos	Cell Signaling	2250
Guinea pig anti-RFP	Abcam Custom preparation, Betley et al., 2013	N/A
Rabbit anti-GFP	Invitrogen	A-11122
Rabbit anti-NPY	Immunostar	22940
Rat anti-GAD65	Custom preparation, Betley et al., 2009	N/A
Guinea pig anti-Vglut2	SYSY	135404
Fluorescein (FITC) AffiniPure Donkey Anti-Sheep IgG (H+L)	Jackson ImmunoResearch Laboratories	713-095-003
Fluorescein (FITC) AffiniPure Donkey Anti-Rabbit IgG (H+L)	Jackson ImmunoResearch Laboratories	711-095-152
Cy3 AffiniPure Donkey Anti-Rabbit IgG (H+L)	Jackson ImmunoResearch Laboratories	711-165-152
Cy3 AffiniPure Donkey Anti-Goat IgG (H+L)	Jackson ImmunoResearch Laboratories	705-165-147
Cy5 AffiniPure Donkey Anti-Goat IgG (H+L)	Jackson ImmunoResearch Laboratories,	705-175-147
Fluorescein (FITC) AffiniPure Donkey Anti-Rat IgG (H+L)	Jackson ImmunoResearch Laboratories	712-095-153
Cy3 AffiniPure Donkey Anti-Rat IgG (H+L)	Jackson ImmunoResearch Laboratories	712-165-153
Fluorescein (FITC) AffiniPure Donkey Anti-Guinea Pig IgG (H+L)	Jackson ImmunoResearch Laboratories	706-095-148
Cy3 AffiniPure Donkey Anti-Guinea Pig IgG (H+L)	Jackson ImmunoResearch Laboratories	706-165-148
Bacterial and Virus Strains		
AAV1.CAGGS.flex.ChR2-tdTomato.WPRE.SV40	University of Pennsylvania Vector Core	AV-1-18917P
AAVrh10.CAGGS.flex.ChR2.tdTomato.WPRE.SV40	University of Pennsylvania Vector Core	AV-10-18917P
AAV1rh.CAG.Flex.eGFP.WPRE.bGH	University of Pennsylvania Vector Core	AV-1-ALL854
AAV1.Syn.Flex.GCaMP6s.WPRE.SV40	University of Pennsylvania Vector Core	AV-1-PV2821
AAV-fDIO-Cre-GFP	University of Pennsylvania Vector Core	N/A
	Custom preparation, Penzo et al., 2015	N/A
pAAV-hSyn-DIO-hM4d(Gi)-mCherry	Krashes et al., 2011	Addgene, 44362
Chemicals, Peptides, and Recombinant Proteins		
Ketoprofen	Santa Cruz Animal Health	sc-363115Rx
Formalin	Sigma-Aldrich	HT50-1-2
Morphine	Sigma-Aldrich	M8777
Freund's Adjuvant, Complete	Sigma-Aldrich	F5881
Lithium chloride	Sigma Aldrich	L9650-100G
Clozapine-N-Oxide	Tocris	4936
NPY	Tocris	1153
Muscimol	Tocris	0289
Baclofen	Tocris	0417
SHU-9119	Tocris	3420
BIBO 3304	Tocris	2412
Saclofen	Sigma-Aldrich	14343
Bicuculline	Sigma-Aldrich	S166
Experimental Models: Cell Lines		
ES cells: 129S6 x C57BL/6J F1 hybrid	Dr. Adam Hantman This paper	N/A

(*Continued on next page*)

Continued

REAGENT or RESOURCE	SOURCE	IDENTIFIER
Experimental Models: Organisms/Strains		
Mouse: Agrp-Ires-cre, Agrp$^{tm1(cre)Lowl}$/J	The Jackson Laboratory	012899
Mouse: Ai32, B6;129S-*Gt(ROSA)26Sor*$^{tm32(CAG-COP4*H134R/EYFP)Hze}$/J	The Jackson Laboratory	012569
Mouse: R26-LSL-Gi-DREADD, B6N.129-Gt(ROSA)26Sor$^{tm1(CAG-CHRM4*,-mCitrine)/Ute}$/J	The Jackson Laboratory	026219
Mouse: VGlut2-IRES-FlpO	Dr. Adam Hantman This paper	N/A
Mouse: Gad2-IRES-FlpO	Dr. Adam Hantman This paper	N/A
Mouse: C57BL/6J	The Jackson Laboratory	000664
Oligonucleotides		
Please see Table S3	N/A	N/A
Software and Algorithms		
SigmaPlot	Systat Software	https://systatsoftware.com
STATISTICA	StatSoft	http://www.statsoft.com/Products/STATISTICA-Features
ANY-Maze	Stoelting	http://www.anymaze.co.uk/index.htm
MATLAB 2016a	MathWorks	https://www.mathworks.com/products/matlab.html
Synapse	Tucker-Davis Technologies	http://www.tdt.com/Synapse/index.html
Other		
Microliter syringe pump, PHD Ultra	Harvard Apparatus	703007
Optogenetic fiber	ThorLabs	FT200UMT
1.25 mm ceramin ferrules	ThorLabs	CFLC230-10
Guide cannulae	Plastics One	8IC315GS5SPC
Internal cannulae	Plastics One	8IC315IS5SPC
Dummy cannulae	Plastics One	8IC315DCSXXC
Dental cement	Lang Dental Manufacturing	B1306,143069
Bone screws	Basi	MF-5182
Optic fibers	Doric	MF2.5, 400/430-0.48
405 nm LED	ThorLabs	M405F1
490 nm LED	ThorLabs	M470F3
Amplifier	Tucker-Davis Technology	RZ5P
Femtowatt photoreceiver	Newport	2151

CONTACT FOR REAGENT AND RESOURCE SHARING

Further information and requests for resources and reagents should be directed to and will be fulfilled by the Lead Contact, J. Nicholas Betley. (jnbetley@sas.upenn.edu).

EXPERIMENTAL MODEL AND SUBJECT DETAILS

Mice were group housed on a 12 h light/12 h dark cycle with *ad libitum* access to food (Purina Rodent Chow, 5001) and water unless otherwise noted. Group housed adult male and female mice (at least 8 weeks old) were used for experimentation. *Agrp-IRES-Cre* (Jackson Labs 012899, *Agrp*$^{tm1(cre)Lowl}$/*J*) (Tong et al., 2008), *Ai32* (Jackson Labs 012569, *B6;129S-Gt(ROSA)26Sor*$^{tm32(CAG-COP4*H134R/EYFP)Hze}$/*J*) (Madisen et al., 2012), *R26-LSL-Gi-DREADD* (Jackson Labs 026219, B6N.129-Gt(ROSA)26Sor$^{tm1(CAG-CHRM4*,-mCitrine)/Ute}$/J) (Zhu et al., 2016), *VGlut2-IRES-FlpO* and *Gad2-IRES-FlpO* generated as described in Method Details, and *C57BL/6J* mice were used for experimentation. Genotyping was performed using primers and conditions provided by Jackson Labs or custom primers for *Gad2-IRES-FlpO* and *VGlut2-IRES-FlpO* mice as described in Method Details. All mice were habituated to handling and experimental conditions prior to experiments. For within-subject behavioral analyses, all mice received all experimental conditions. For between-subject analyses, mice were randomly assigned to experimental condition. We

performed experiments in both male and female subjects, and did not observed any trends or significant sex differences. Thus, to ensure our studies were appropriately powered and to minimize the number of subjects who had to undergo pain assays, we combined males and females for analyses in all experiments. All procedures were approved by the University of Pennsylvania Institutional Animal Care and Use Committee.

METHOD DETAILS

Recombinant Adeno-Associated Virus (rAAV) Constructs and Production:

The following Cre- or FlpO-dependent rAAV vectors were used: AAV1.CAGGS.Flex.ChR2-tdTomato.WPRE.SV40 (titer: 1.38e13 GC/ml), AAVrh10.CAGGS.flex.ChR2.tdTomato.WPRE.SV40 (titer: 1.23e13 GC/ml), AAV1rh.CAG.Flex.eGFP.WPRE.bGH (titer: 1.708e13 GC/ml), AAV1.Syn.Flex.GCaMP6s.WPRE.SV40 (titer: 4.216e13 GC/ml), AAV-fDIO-Cre-GFP (titer: 2.91e13 GC/ml), pAAV-hSyn-DIO-hM4D(Gi)-mCherry (titer: 4.3e12 GC/ml). All viruses were produced by the University of Pennsylvania Vector Core, except for the latter which was purchased from Addgene (ID 44362). CAG, promoter containing a cytomegalovirus enhancer; the promoter, first exon and first intron of the chicken beta actin gene; and the splice acceptor of rabbit beta-globin gene. Syn, human Synapsin 1 promoter. FLEX, Cre-dependent flip-excision switch. WPRE, woodchuck hepatitis virus response element. bGH, bovine growth hormone polyadenylation signal. ChR2, channelrhodopsin-2. GCaMP, Genetically encoded calcium indicator resulting from a fusion of GFP, M13 and Calmodulin. DIO, Double-floxed inverted oreientation. hM4, human M4 muscarinic receptor.

Generation of FlpO mice:

VGlut2-IRES-FlpO mouse generation. Targeting vector construction: The targeting vector was constructed using a recombineering technique previously described (Liu et al., 2003). A 8,572 bp genomic DNA fragment containing exon 9-12 of the VGlut2 gene was retrieved from BAC clone RP23-228J18 to a vector containing the DT gene, a negative selection marker. A cassette of IRES-FlpO-loxP2272-ACE-Cre POII NeoR-loxp2272 was inserted between stop codon TAA and 3′ UTR. The length of the 5′ homologous arm is 5,519 bp and that for the 3′ arm is 3,049 bp. ES cell targeting and screening: The targeting vector was electroporated into F1 hybrid of 129S6 x C57BL/6J ES cells derived by the Janelia Transgenic Facility. The G418 resistant ES clones were screened by nested PCR using primers outside the construct paired with primers inside the inserted cassette. The primer sequences were as follows: 5′ arm forward primers: VGlut2 Scr F1 (5′-CAGCTCCTTTGAGAATGGCA-3′) and VGlut2 Scr F2 (5′- CCTGACAGTTTCAAAACGTGG-3′). Reverse primers: IRES R1 (5′-AGGAACTGCTTCCTTCACGA-3′) and IRES R2 (5′-CCTAGGAATGCTCGTCAAGA-3′). 3′ arm forward primers: ACE F3 (5′-ACAGCACCATTGTCCACTTG-3′) and ACE F4, (5′-GCTGGTAAGGGATATTTGCC-3′); Reverse primers: VGlut2 Scr R3 (5′-ACATTGGTGCCACTTAGCTG-3′) and VGlut2 Scr R4 (5′- GCATGTGAGCTACCTTAAGC-3′). *Generation of chimera and F1 genotyping:* The PCR positive ES clones were expanded for generation of chimeric mice. The ES cells were aggregated with 8-cell embryos of CD-1 strain. The chimeras were mated with wild-type C57BL/6J females and the neo cassette was automatically removed in F1 pups. The F1 pups were genotyped by PCR using primers flanking the insertion site and a primer in IRES for the 5′ arm. The primer set VGlut2 gt F P1 (5′-TGCTACCTCACAGGAGAATG-3′) and IRES P3 (5′-GCTTCGGCCAGTAACGTTAG-3′). The PCR products are 186 bp for the mutant allele. The primer set for the 3′ arm is VGlut2 P2 (5′- TGACAACTGCCACAGATTG-3′) and FlpO gt F P4 (5′-CTGGACTACCTGAGCAGCTA-3′). The generated PCR products are 294 bp for the mutant allele. The primer set VGlut2 P1 (5′-TGCTACCTCACAGGAGAATG-3′) and Vglut2 P2 (5′-TGACAACTGCCACAGATTG-3′) is designed to detect the wild-type allele for homozygote genotyping. The correct targeting was further confirmed by obtaining homozygotes from chimera x F1 heterozygous females mating. The mouse lines from two independent ES cell clones were homozygosity tested and bred for experiments. Genotyping PCR: The template DNA was obtained by digesting an ear piece in 50 μL proteinase K buffer (50 mM Tris pH 8.8, 1 mM EDTA pH 8.0, 0.5% Tween-20 and proteinase K 0.6 mg/ml). The reaction was incubated at 55°C overnight and heat inactivated at 100°C for 10 minutes. 0.5 μL of the template was used in 12 μL PCR reaction. The reaction was carried out with an initial denature cycle of 94°C for 3 min, followed by 35 cycles of 94°C 30 s, 55°C 30 s and 72°C 30 s and ended with one cycle of 72°C for 5 min.

Gad2-IRES-FlpO mouse generation. Targeting vector construction: The targeting vector was constructed using a recombineering technique previously described (Liu et al., 2003). A 10,389 bp genomic DNA fragment containing exon 16 of the Gad2 gene was retrieved from BAC clone RP23-27D24 to a vector containing the DT gene, a negative selection marker. A cassette of IRES-FlpO-loxP2272-ACE-Cre POII NeoR-loxp2272 was inserted between stop codon TAA and 3′ UTR. The length of the 5′ homologous arm is 3,195 bp and that for the 3′ arm is 7,193 bp. *ES cell targeting and screening:* The targeting vector was electroporated into F1 hybrid of 129S6 x C57BL/6J ES cells derived by the Janelia Transgenic Facility. The G418 resistant ES clones were screened by nested PCR using primers outside the construct paired with primers inside the inserted cassette. The primer sequences were as follows: 5′ arm forward primers: Gad2 Scr F1 (5′-CAATTGCTGAGCTGAAGTGC-3′) and Gad2 Scr F2 (5′-CAAGCAGTCAGCA GATTCCA-3′). Reverse primers: IRES R1 (5′-AGGAACTGCTTCCTTCACGA-3′) and IRES R2 (5′-CCTAGGAATGCTCGTCAAGA-3′). *3′ arm forward primers:* ACE F3 (5′- ACAGCACCATTGTCCACTTG −3′) and ACE F4 (5′-GCTGGTAAGGGATATTTGCC-3′); Reverse primers: Gad2 Scr R3 (5′-GGCTTGATTCCTCAGAGGAA-3′) and Gad2 Scr R4 (5′-GCACAACAGTTGGACCTTAG-3′). *Generation of chimera and F1 genotyping:* The PCR positive ES clones were expanded for generation of chimeric mice. The ES cells were aggregated with 8-cell embryos of CD-1 strain. The chimeras were mated with wild-type C57BL/6J females and the neo cassette was automatically removed in F1 pups. The F1 pups were genotyped by PCR using primers flanking the insertion site and a primer in IRES for the 5′ arm. The primer set Gad2 gt F P1 (5′-TATGGGACCACAATGGTCAG-3′) and IRES P3 (5′-GCTTCGGCCAGTAACGTTAG-3′).

The PCR products are 212 bp for the mutant allele. The primer set for the 3′ arm is Gad2 P1 (5′-TATGGGACCACAATGGTCAG-3′), Gad2 P2 (5′- TGCTGGGATTAAAGGCATGC-3′) and FlpO gt F P4 (5′-CATCAACAGGCGGATCTGAT-3′). The generated PCR products are 261 bp for the mutant allele and 325 bp for wild-type allele. The correct targeting was further confirmed by obtaining homozygotes from chimera x F1 heterozygous females mating. The mouse lines from three independent ES cell clones were homozygosity tested and were bred for experiments. *Genotyping PCR:* Genotyping PCR was performed as for *VGlut2-IRES-FlpO* mice.

Viral Injections, Fiber Optic and Cannula Placement:

Bilateral viral injections and unilateral implantation of ferrule-capped optical fibers (200 μm core, NA 0.37 for optogenetic stimulation; 400 μm core, NA 0.48 for fiber photometry, Doric) were performed as previously described (Betley et al., 2013). For somatic stimulation of AgRP neurons, *Agrp-IRES-Cre* mice were crossed with *Ai32* mice to express ChR2 in AgRP neurons. Mice were anesthetized with isoflurane (1.5%–3%), given ketoprofen (5 mg/kg) and bupivacaine (2 mg/kg) analgesia and placed into a stereotaxic device (Stoelting). An optical fiber was placed over the arcuate hypothalamic nucleus (ARC) at bregma −1.35 mm, midline ± 0.25 mm, skull surface −5.8 mm. For axonal stimulation of AgRP neurons, a rAAV encoding Cre-dependent ChR2 was bilaterally injected into the ARC of *AgRP-IRES-Cre* mice using the aforementioned ARC injection coordinates (150 nL per site, bilaterally). Optical fibers were unilaterally implanted according to the following coordinates. BNST: bregma +0.85 mm, midline ± 0.82 mm, skull surface −3.8 mm; PVH: bregma −0.5 mm, midline ± 0.2 mm, skull surface −5.4 mm; PVT: bregma −1.0 mm, midline ± 0.0 mm, skull surface −2.7 mm; LH: bregma −1.0 mm, midline ± 0.9 mm, skull surface −5.4 mm; CeA: bregma −1.15 mm, midline ± 2.4 mm, skull surface −4.25 mm; ARC: bregma −1.35 mm, midline ± 0.25 mm, skull surface −5.8 mm; PAG: bregma −4.4 mm, midline ± 0.6 mm, skull surface −2.8 mm; lateral PBN: bregma −5.8 mm, midline ± 1.2 mm, skull surface −3.7 mm. Fibers were secured to the skull with bone screws and dental cement. For pharmacological experiments, mice were implanted with unilateral 26 gauge guide cannulae (Plastics One, Roanoke, VA) above the lateral PBN (according to the above coordinates) which were secured to the skull with bone screws and dental cement (Alhadeff et al., 2015). For chemogenetic inhibition of lateral PBN neurons, VGlut2-IRES-FlpO and Gad2-IRES-FlpO mice were bilaterally injected (200 nl/hemisphere) in the lateral PBN with a FlpO-dependent rAAV encoding Cre, and a Cre-dependent rAAV encoding inhibitory Designer Receptors Exclusively Activated by Designer Drugs (DREADDs, hM4D). For fiber photometry, a rAAV encoding Cre-dependent GCaMP6s was bilaterally injected into the ARC of *AgRP-IRES-Cre* mice using the following coordinates: bregma −1.35 mm; midline ± 0.25 mm; skull surface −6.15 mm and −6.3 mm (250 nL per site, bilaterally), and an optical fiber was implanted over the ARC using the following coordinates: bregma −1.35 mm; midline ± 0.25 mm; skull surface −6.0 mm. Mice were given at least 3 weeks for recovery and transgene expression. Fiber and cannula placements were verified post-mortem.

General Experimental Design:

For each experiment, our subject numbers were determined by our pilot studies, laboratory publications, and power analyses [power = 0.8, significance level = 0.05, effect sizes = 10%–30%]. For within-subject behavioral and fiber photometry analyses, all mice received all experimental conditions. For between-subject analyses, mice were randomly assigned to experimental condition. For all behavioral and fiber photometry experiments, experiments were performed in at least two cohorts to ensure replicability of results, by at least 2 researchers who were blinded to experimental conditions. For histological experiments, protein intensities and neuron counts were quantified by 4 research assistants who were blinded to experimental condition. For all behavioral and fiber photometry experiments, virus expression, fiber placements, and/or cannula placements were verified post-mortem, and any mice with viral expression or implants outside of the area of interest were excluded from all analyses.

In Vivo Photostimulation:

Photostimulation was performed as previously described (Betley et al., 2013), with 10 ms pulses at 20 Hz for 1 s, repeated every 4 s. The output beam from a diode laser (450 nm, Opto Engine) was controlled by a microcontroller (Arduino Uno) running a pulse generation script. The laser was coupled to a multimode optical fiber (200 μm core, NA 0.37, Doric) with a 1.25 mm OD zirconium ferrule (Kientech) and mating sleeve that allowed delivery of light to the brain by coupling to the implanted ferrule-capped optical fiber in the mouse. Power was set to ensure delivery of at least 2 mW/mm^2 to AgRP soma and at least 5 mW/mm^2 to the center of the AgRP neuron projection fields.

Food Deprivation/Restriction:

For 24 h food deprivation, mice were placed in a cage with alpha dry bedding and *ad libitum* access to water, but no food, 24 h prior to experimentation. For chronic food restriction, mice were weighed at the same time each day and given chow once daily (1.5–3.0 g) after experimentation to maintain 85%–90% of their starting body weight.

Food Intake Experiments:

Effects of AgRP neuron stimulation on food intake. Mice were allowed to habituate for at least one hour to a chamber with a lined floor and ad libitum access to chow and water. Following the habituation period, food intake was measured for 1 h to establish a pre-stimulation baseline. Photostimulation was performed during the next hour. After each hour, food intake was measured. For somatic AgRP neuron stimulation, only mice that consumed > 0.6 g of chow were included in experiments. Food intake evoked by stimulation of each AgRP neuron projection subpopulation was measured and reported in Figure S3D.

Effects of AgRP neuron inhibition on food intake. Mice were habituated to an empty home cage with a lined floor. Mice were food deprived for 24 h, intraperitoneally (i.p.) injected with saline or clozapine-N-oxide (CNO, 2.5 mg/kg, Tocris), and placed into their cage with ad libitum access to chow and water. Chow intake was measured 4 h post-injection, accounting for crumbs.

Effects of hotplate exposure on latency to feed. 24 h food deprived mice were individually placed in a home cage with a lined floor and access to water. After a 10-min habituation period, mice were exposed to a cast iron plate at either 25°C or 52°C for 1 min and immediately placed back into the cage with food and water. Latency to consume food was measured.

Effects of formalin injection on food intake. 24 h food deprived mice were individually placed in a home cage with a lined floor and access to water. After a 10-min habituation period, mice were injected subcutaneously in the dorsal hindpaw with saline or 2% formalin (20 μl, Sigma HT50-1-2) and returned to their cage with food. Food intake was recorded 1 h post-injection.

Inflammatory Pain Measurements (Formalin Test):

Mice were placed in a clear enclosure for a 10-min habituation period. Mice were subcutaneously injected in the dorsal hindpaw with saline or 2% formalin (20 μl). Mice were monitored for time spent licking paw, and number of lick bouts, for 1 h post-injection by researchers blinded to experimental condition. All sessions were video-recorded. The time spent paw licking was grouped into 5-min bins (Hunskaar and Hole, 1987) and recorded for 1 h. Additionally, acute (0-5 min) and inflammatory (15-45 min) phase pain responses were quantified.

Effects of ketoprofen on formalin test:

The non-steroidal anti-inflammatory drug ketoprofen (30 mg/kg) or saline was administered subcutaneously 30 min before formalin injection.

Effects of food deprivation on formalin test:

Food was removed 24 h prior to formalin injection. *Ad libitum* fed mice served as controls.

Effects of formalin on paw inflammation:

24 h food deprived mice were lightly anesthetized and paw circumference was measured immediately before saline or formalin paw injection. Paw circumference was measured again 30 min post-injection.

Optogenetic AgRP neuron stimulation:

To assess the effects of AgRP neuron stimulation on acute and inflammatory phase pain responses to formalin, mice received optogenetic stimulation of AgRP neurons or individual projection subpopulations beginning 10 min prior to formalin injection and lasting throughout the formalin test. To assess the ability of AgRP neuron stimulation to affect an ongoing inflammatory pain response, stimulation of AgRP neurons or AgRP→PBN neurons was initiated 25 min post-formalin injection and lasted for the duration of the formalin test. To assess whether the offset of AgRP→PBN neuron activity results in a reinstatement of inflammatory phase pain response, laser stimulation was given 10 min prior to formalin injection and terminated 25 min post-formalin injection. To test whether prolonged AgRP→PBN neuron stimulation affects the ability to paw lick, mice were stimulated for 40 min and formalin-induced acute phase pain was measured.

Chemogenetic AgRP neuron inhibition:

To assess the necessity of AgRP neuron activity for the inhibition of inflammatory pain by hunger, mice were 24 h food deprived and i.p. injected with CNO (2.5 mg/kg) 15 min before formalin injection.

Chemogenetic inhibition of lateral PBN VGlut2 and Gad2 neurons:

To determine whether lateral PBN glutamatergic (VGlut2-expressing) or GABAergic (Gad2-expressing) neurons mediate inflammatory pain responses, VGlut2^{hM4D}, Gad2^{hM4D}, and control mice were i.p. injected with CNO (2.5 mg/kg) 15 min before formalin injection.

Thermal Pain Measurements (Hotplate Test):

A cast iron plate with plexiglass walls was placed on a hotplate and heated to 52°C. Mice were placed on the hotplate and latency to withdraw paw was recorded by researchers blinded to experimental condition. All sessions were video-recorded.

Effects of morphine on hotplate test:

Mice underwent a baseline hotplate test and were subsequently i.p. injected with saline or morphine (10 mg/kg). Mice were tested again on the hotplate 30 min post-injection.

Effects of food deprivation on hotplate test:

Food was removed 24 h prior to hotplate test. *Ad libitum* fed mice served as controls.

Optogenetic AgRP neuron stimulation during hotplate test:

To assess the effects of AgRP neuron stimulation on acute thermal pain response, mice were placed in a plexiglass chamber, attached to patch fibers, and allowed to habituate for 30 min. Mice underwent a baseline hotplate test, and 5 min later laser stimulation was initiated. Mice were tested again on the hotplate following 15 and 45 min of stimulation of AgRP neurons or control light delivery to GFP-expressing mice. A separate experiment was performed to assess the role of AgRP→PBN neurons on acute thermal pain by delivering light to the PBN of mice expressing either ChR2 or GFP in AgRP neurons, using identical experimental procedures.

Mechanical Pain Measurements (Von Frey Test):

Mice were habituated for 30 min in small plexiglass chambers atop mesh flooring. Twelve Von Frey filaments (ranging from 0.008 g to 6 g) were used. Starting with the smallest Von Frey filament and continuing in ascending order, each filament was applied to the plantar surface of the hind paw until the filament bent. Each filament was tested 5 times. The number of withdrawal responses was recorded for each filament, and the percentage withdrawal responses for each filament was calculated (# of withdrawal trials/total trials). Withdrawal threshold was determined as the filament at which the mouse responded with a paw withdrawal to > 50% of trials. To test the effects of hunger on mechanical pain, mice were 24 h food deprived and then subjected to the Von Frey test.

Inflammation-Induced Sensitization:

Complete Freund's Adjuvant (CFA, Sigma) was diluted 1:1 in saline and injected (20 μl) into the plantar surface of the paw after a baseline Von Frey or hotplate test. Given that we and others observe a more robust CFA-induced sensitization to thermal pain at 55°C (Carey et al., 2017), we used this temperature for CFA-induced thermal sensitization. Von Frey or hotplate tests were repeated 3 h, 24 h, and 48 h post-CFA injection.

Effects of hunger on inflammation-induced sensitization:

Mice were 24 h food deprived and subjected to Von Frey or hotplate tests as described above. Mice were provided enough food in one daily aliquot to maintain 85%–90% BW through the rest of testing (up to 48 h post-CFA injection).

Effects of AgRP neuron stimulation on inflammation-induced sensitization:

Optogenetic AgRP neuron stimulation was performed for 1 h before each of the post-CFA Von Frey tests (3 h, 24 h, and 48 h post-CFA injection).

Conditioned Place Avoidance:

Two-sided apparatus were used with distinct visual (black versus white walls), textural (flooring: plastic versus soft textural side of Kimtech bench-top protector), and olfactory (almond versus peppermint extract) cues. A neutral middle zone to shuttle between sides was maintained and the chamber was equipped with an overhead camera to track mouse position. *Ad libitum* fed mice were habituated to the apparatus and a pre-conditioning preference was determined via AnyMaze software. Mice were then separated into two groups: food restricted (85%–90% of initial body weight) or *ad libitum* fed. Conditioning, which consisted of a saline paw injection (20 μl) on the less preferred side or a 2% formalin paw injection (20 μl) on the preferred side was performed twice daily for four days. To isolate conditioning to the inflammatory phase of formalin pain, mice were placed in the apparatus 15 min post-injection. After conditioning, all mice were given *ad libitum* access to food. The next day, mice were given access to both sides of the apparatus and their position and activity were tracked. The percentage occupancy, shifts in occupancy, and total distance traveled in the formalin-paired side during the post-conditioning test were calculated. To control for any associative learning deficits during hunger, the same conditioned place avoidance paradigm was used, except that mice were given i.p. saline on the less preferred side and i.p. lithium chloride (125 mg/kg) on the preferred side during conditioning.

Locomotor Activity Assays:

Effects of food deprivation of formalin-induced immobility. Mice were habituated to 10'' x 10'' x 10'' plexiglass chambers. Food was removed from mice 24 h prior to 2% formalin injection, and mice were placed in chambers and video-recorded during the inflammatory phase following formalin injection (15-45 min post-injection). Videos were analyzed with AnyMaze software (Stoelting) for time spent immobile, which was defined as not changing position in the X-Y grid for at least 8 s.

Effects of AgRP→PBN neuron stimulation on locomotor activity. Mice were habituated to 10'' x 10'' x 10'' plexiglass chambers. AgRP→PBN neurons were optogenetically stimulated for 30 min and behavior was video-recorded. Videos were analyzed with AnyMaze software (Stoelting) for total distance traveled and time spent immobile, which was defined as not changing position in the X-Y grid for at least 8 s.

Immunohistochemistry and Imaging:

Mice were transcardially perfused with 0.1 M phosphate buffered saline (PBS) followed by 4% paraformaldehyde (PFA). Brains were removed and post-fixed for 4 h in PFA and then washed overnight in PBS. Coronal brain sections were cut (30-200 μm sections) on a vibratome or cryostat and stored in PBS. Brain sections were incubated overnight at 4°C with primary antibodies diluted in PBS, 1% BSA and 0.1% Triton X-100. Antibodies used: goat anti-AgRP (1:2,500, Neuromics, GT15023), rabbit anti-cFos (1:5,000, Cell Signaling, 2250), guinea pig anti-RFP (1:10,000) (Betley et al., 2013), rabbit anti-GFP (1:5,000, Invitrogen, A-11122), rabbit anti-NPY (1:1,500, Immunostar, 22940), rat anti-GAD65 (1:2,000) (Betley et al., 2009), guinea pig anti-VGlut2 (1:2,000, SYSY, 135404). Sections were washed 3 times and incubated with species appropriate and minimally cross-reactive fluorophore-conjugated secondary antibodies (1:500, Jackson ImmunoResearch) for 2 h at room temperature. Sections were washed twice with PBS and mounted and coverslipped with Fluorogel. Epifluorescence images were taken on a Leica stereoscope to verify fiber placements, cannula placements, and obtain low magnification images. Confocal micrographs were taken on a Leica STED laser scanning microscope using a 20X, 0.75 NA objective for quantification of Fos immunoreactivity under AgRP axons; a 40X, 1.3 NA objective for quantification of protein expression in AgRP→PBN terminals; and a 63X or 100X, 1.4 NA objective for protein colocalization of mCherry, VGlut2, and GAD65 in PBN axon terminals.

Quantification of Protein Expression:

Immediate early gene protein expression analysis. To quantify the number of neurons expressing Fos protein under AgRP axons, mice received no treatment (n = 3) or a 20 μL subcutaneous injection of formalin (5%, n = 3) or saline (n = 3) in the dorsal hindpaw. Two hours later, mice were perfused and brains were processed for immunohistochemistry. First, images of Fos and AgRP from a formalin-treated mouse were obtained in each of the major AgRP projection target regions. Identical image acquisition settings were maintained for all subsequent imaging of Fos and AgRP in experimental and control mice. To quantify the number of Fos-expressing neurons in each AgRP neuron target region, single optical sections (pinhole = 1 airy unit, 2-4 sections/mouse/AgRP target region) were used and the AgRP neuron staining was used to define the region for quantification (see Figure 4A).

Quantification of synaptic protein expression. Ad libitum fed (n = 2) and 24 h food deprived (n = 3) mice were perfused and PBN brain sections were processed for NPY, the GABA synthetic enzyme GAD65, and AgRP immunoreactivity. Confocal images were obtained first from a food deprived mouse so that the intensities of NPY, GAD65, and AgRP were in the linear range. Image acquisition settings were maintained for all subsequent imaging and 2 PBN images per mouse were obtained. For intensity quantifications, single confocal sections (pinhole = 1 airy unit) were used and the intensities of NPY, GAD65, and AgRP were calculated using the histogram function on Adobe Photoshop.

Colocalization of hM4D, Vglut2, and GAD65 in lPBN neurons. To determine the specificity of expression of hM4D in the *Gad2-IRES-FlpO* and *Vglut2-IRES-FlpO* knock-in lines, staining was performed against mCherry, Vglut2 and GAD65 in coronal sections from at least 2 mice/line used for experimentation. For quantification, single confocal sections (pinhole = 1 airy unit) were used and the number of Vglut2+ or GAD65+ structures that expressed hM4D-mCherry were counted.

Pharmacology:

For all experiments, mice were habituated to handling and infusion procedures. Drugs were diluted from frozen aliquots before each experiment and microinjected (100 nl) with a Hamilton syringe attached to an internal cannula (Plastics One) and microliter syringe pump (PHD Ultra, Harvard Apparatus) into the PBN of mice immediately before a formalin test (see above) or food intake measurements.

Effects of lPBN NPY, GABA agonists, and AgRP analog on formalin-induced inflammatory pain:

Neuropeptide Y [NPY, Tocris, 0.1 μg], $GABA_A$ and $GABA_B$ receptor agonists [muscimol, Tocris, 25 ng and baclofen, Tocris, 25 ng], an AgRP analog [melanocortin 4 receptor antagonist; SHU9119, 25 pmol] or vehicle [artificial cerebrospinal fluid (aCSF)] was microinjected into the lateral PBN immediately before paw injection of formalin.

Effects of lPBN NPY, GABA agonists, and AgRP analog on food intake:

The aforementioned drugs were infused in the lPBN during the light cycle and food intake was recorded 1 h post-injection.

Effects of locus coeruleus NPY on formalin-induced inflammatory pain:

Since AgRP axons terminate both in the lPBN and the locus coeruleus, NPY or vehicle was infused in the locus coeruleus area (directly medial from lPBN) immediately before formalin paw injection.

Effects of lPBN NPY Y1 receptor antagonist on the inhibition of inflammatory pain by hunger:

Microinjections of the selective NPY Y1 receptor antagonist BIBO 3304 [Tocris, 3 μg], $GABA_A$ and $GABA_B$ antagonists [saclofen, 100 ng, Sigma, and bicuculline, 10 ng, Sigma] or vehicle (50% DMSO in aCSF) were infused into the lPBN of 24 h food deprived mice.

Effects of lPBN NPY Y1 receptor antagonist on the inhibition of inflammatory pain by AgRP→PBN stimulation:

To test whether the protective effects of AgRP→PBN neuron stimulation on inflammatory pain are mediated by NPY, we performed an experiment similar to that in (Atasoy et al., 2012). Mice expressing ChR2 in AgRP neurons were injected in the lPBN with vehicle or the Y1 receptor antagonist BIBO 3304. An optic fiber was then inserted through the PBN cannula and a formalin paw injection was administered. AgRP→PBN stimulation occurred throughout the duration of the formalin test.

Fiber Photometry:

Food-restricted (85%–90% body weight) mice in their home cage were attached to a patch fiber (400 μm core, NA 0.48, Doric) and connected to 405 nm and 490 nm LEDs (Thor Labs, M405F1, M470F3) modulated by a real-time amplifier [Tucker-Davis Technology (TDT), Alachua, FL, RZ5P] and focused onto a femtowatt photoreceiver (Newport, Model 2151) (Figure 6C) (Gunaydin et al., 2014). Changes in calcium-dependent GcaMP6s fluorescence (490 nm) signal were compared with calcium-independent GCaMP6s fluorescence (405 nm), providing internal control for movement and bleaching artifacts (Lerner et al., 2015; Su et al., 2017). Fluorescence measurements (1 Hz) were extracted from Synapse software (TDT), processed in MATLAB (GraphPad), and expressed as ΔF/F, where the denominator represents average baseline fluorescence.

Effects of acute thermal pain on AgRP neuron activity:

Food restricted (85%–90% BW) mice were connected to the fiber photometry setup for a 5-min baseline period in their home cage. Mice were then placed on a 25°C or 52°C plate for 1 min, after which they returned to their cage. GCaMP6s fluorescence was monitored for 10 min following hotplate exposure.

Effects of acute and inflammatory formalin-induced pain on AgRP neuron activity:
Food restricted (85%–90% BW) mice were connected to the fiber photometry setup for a 5 min baseline period in their home cage. Mice were injected in the dorsal hindpaw with 2% formalin or saline (20 μl) and returned to their cage. GCaMP6s fluorescence was monitored for 1 h post-formalin injection.

QUANTIFICATION AND STATISTICAL ANALYSIS

Data were expressed as means ± SEMs in figures and text. Paired or unpaired two-tailed t tests with or without Bonferroni corrections and Pearson regressions were performed as appropriate. One-way, two-way, and repeated-measures ANOVA were used to make comparisons across more than two groups using SigmaPlot or STATISTICA. Test, statistics, significance levels, and sample sizes for each experiment are listed in Tables S1 and S2. ns $p > 0.05$, t tests and post hoc comparisons: *$p < 0.05$, **$p < 0.01$, ***$p < 0.001$; interaction: ∞$p < 0.05$, ∞∞$p < 0.01$, ∞∞∞$p < 0.001$; main effect (group, condition or drug): ☼< 0.05, ☼☼$p < 0.01$, ☼☼☼$p < 0.001$.

Cell

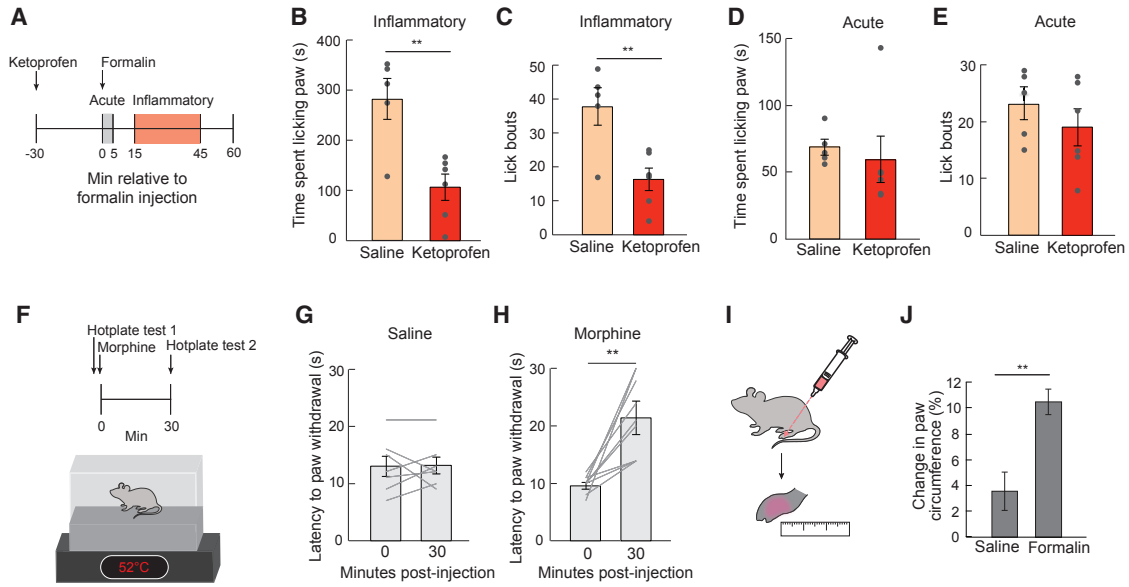

Figure S1. Anti-inflammatory and Opiate Drug Administration Reduce Responses to Inflammatory Phase and Thermal Pain, Respectively, Related to Figure 1

(A) Experimental timeline for effects of an anti-inflammatory analgesic (ketoprofen) on the formalin test.

(B) Inflammatory phase formalin-induced paw licking (time) in i.p. saline- (n = 5) and ketoprofen- (n = 6) treated mice (unpaired t test, $p < 0.01$).

(C) Inflammatory phase formalin-induced lick bouts in saline- and ketoprofen-treated mice (unpaired t test, $p < 0.01$).

(D) Acute phase formalin-induced paw licking (time) in saline- and ketoprofen-treated mice (unpaired t test, p = ns).

(E) Acute phase formalin-induced lick bouts in saline- and ketoprofen-treated mice (unpaired t test, p = ns).

(F) Experimental timeline for effects of morphine on the hotplate test.

(G) Latency to paw withdrawal from 52°C hotplate before and 30 min post i.p. saline injection (paired t test, p = ns).

(H) Latency to paw withdrawal from hotplate before and 30 min post i.p. morphine injection (paired t test, $p < 0.01$).

(I) Experimental design: 24 h food deprived mice were injected with saline or formalin in their hindpaw and change in paw circumference was measured 30 min post-injection.

(J) Change in paw circumference in food deprived saline- (n = 6) and formalin- (n = 9) injected mice (unpaired t test, $p < 0.01$).

Data are expressed as mean ± SEM, ns $p > 0.05$, t tests: **$p < 0.01$. See also Table S2.

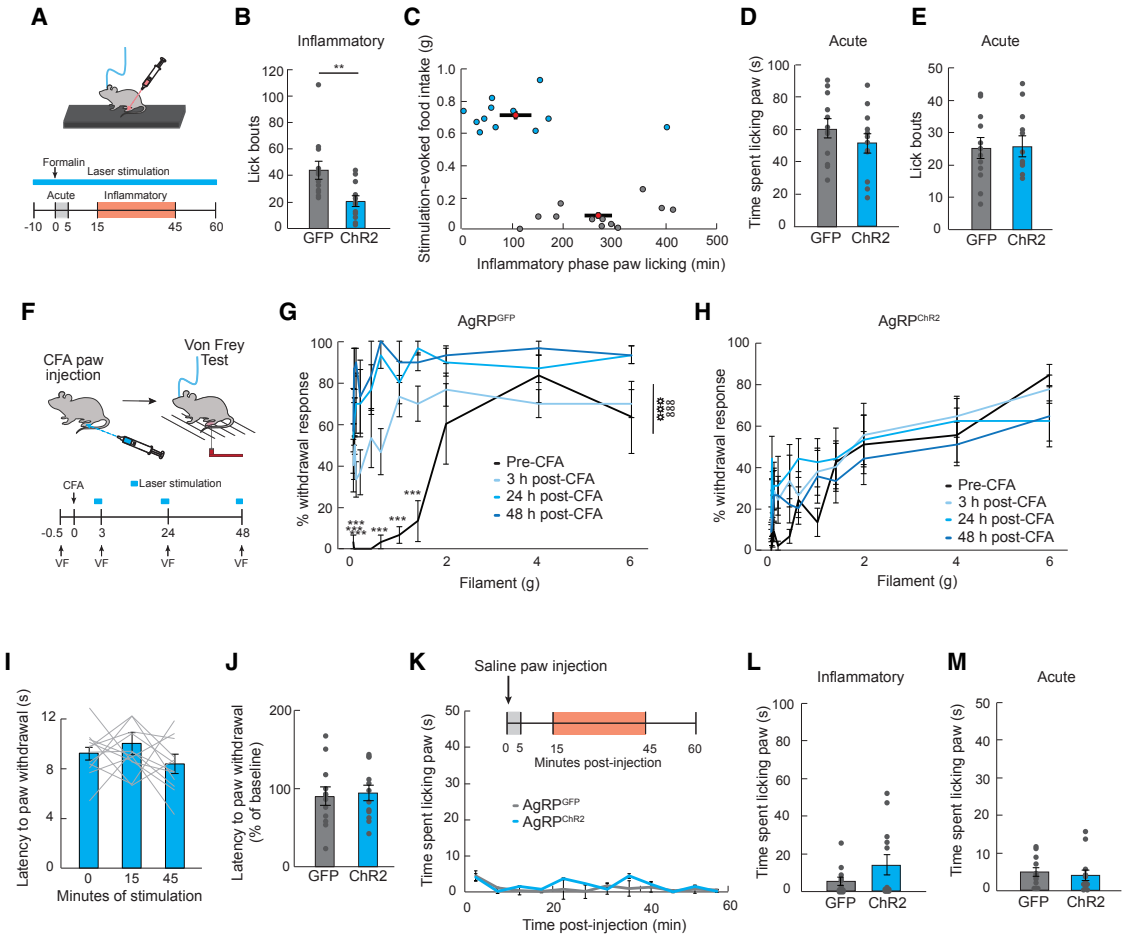

Figure S2. AgRP Neuron Activity Specifically Inhibits Inflammatory Phase Pain Response without Off-Target Licking Effects, Related to Figure 4

(A) Experimental design: Laser light pulses delivered to AgRP neurons of AgRP^{GFP} and AgRP^{ChR2} mice began 10 min before formalin injection and continued while formalin-induced paw licking was quantified.

(B) Inflammatory phase formalin-induced lick bouts in AgRP^{GFP} and AgRP^{ChR2} mice (unpaired t test, $p < 0.01$).

(C) Laser stimulation-induced food intake (y axis) correlates with inflammatory phase paw licking (x axis); AgRP^{GFP} (gray circles, n = 12), AgRP^{ChR2} (blue circles, n = 12), red circles are group averages (Pearson regression, R = 0.60, $p < 0.01$).

(D) Time spent paw licking during acute phase of formalin test in AgRP^{GFP} and AgRP^{ChR2} mice (unpaired t test, p = ns).

(E) Acute phase formalin-induced lick bouts in AgRP^{GFP} and AgRP^{ChR2} mice (unpaired t test, p = ns).

(F) Experimental design: AgRP^{GFP} and AgRP^{ChR2} mice were injected with Complete Freund's Adjuvant (CFA) after a baseline Von Frey test. Mice underwent additional Von Frey tests at 3h, 24 h, and 48 h post-CFA injection, with 1 h of laser stimulation before each test.

(G) Percentage withdrawal from Von Frey Filaments before and 3 h, 24 h, and 48 h post-CFA injection in AgRP^{GFP} mice (n = 6, two-way repeated-measures ANOVA, $p < 0.001$).

(H) Percentage withdrawal from Von Frey Filaments before and 3 h, 24 h, and 48 h post-CFA injection in AgRP^{ChR2} mice (n = 9, two-way repeated-measures ANOVA, p = ns).

(I) Latency to withdraw paw from hotplate during AgRP neuron stimulation in AgRP^{ChR2} mice (n = 12, repeated-measures one-way ANOVA, p = ns).

(J) Normalized latency to withdraw paw from hotplate in AgRP^{GFP} and AgRP^{ChR2} mice after 45 min of laser stimulation (unpaired t test, p = ns).

(K) Time spent licking paw in AgRP^{GFP} (n = 12) and AgRP^{ChR2} (n = 12) mice with laser stimulation following saline paw injection (two-way repeated-measures ANOVA, p = ns).

(L) Inflammatory phase paw licking (time) in AgRP^{GFP} and AgRP^{ChR2} mice during laser stimulation following saline paw injection (unpaired t tests, p = ns). (M) Acute phase paw licking (time) in AgRP^{GFP} and AgRP^{ChR2} mice during laser stimulation following saline paw injection (unpaired t tests, p = ns).

Data are expressed as mean ± SEM, ns $p > 0.05$, t tests and post hoc comparisons: *$p < 0.05$, **$p < 0.01$, ***$p < 0.001$; ANOVA interaction: ∞$p < 0.05$, ∞∞∞$p < 0.001$; ANOVA main effect of drug: ☼☼☼$p < 0.001$. See also Table S2.

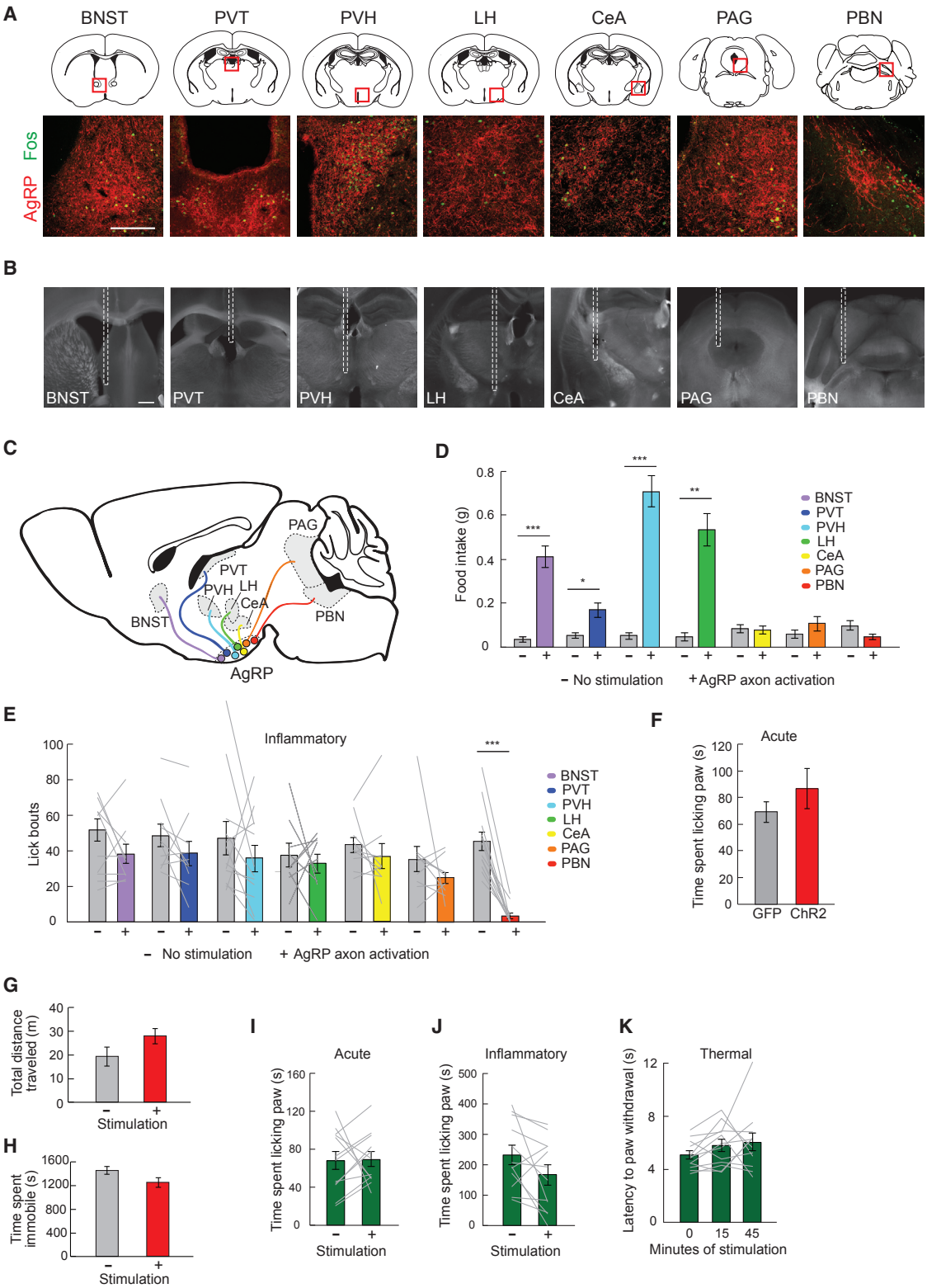

Figure S3. AgRP → PBN Neurons Selectively Mediate Inflammatory Pain, Related to Figure 4

(A) Schematics of target brain regions and representative images of formalin-induced Fos underlying AgRP axon projections in the BNST, PVT, PVH, LH, CeA, PAG, and PBN. Scale bar, 150 μm.

(legend continued on next page)

(B) Representative images of fiber placements (indicated in white dotted lines. Scale bar, 1 mm.
(C) Diagram of the major AgRP neuron projection subpopulations analyzed.
(D) Food intake (1 h) in *ad libitum* fed mice with (+, colored bars) and without (-, gray bars) laser stimulation of AgRP axons (n = 9-12/target region, paired t test with Bonferroni correction, BNST and PVH $p < 0.001$; LH $p < 0.01$, PVT $p < 0.05$; CeA, PAG, PBN p = ns).
(E) Inflammatory phase formalin-induced lick bouts with (+, colored bars) and without (-, gray bars) AgRP neuron stimulation of discrete AgRP projection subpopulations (n = 9-12/target region, paired t tests with Bonferroni correction, all p values = ns except for PBN, $p < 0.001$).
(F) Acute phase formalin-induced paw licking (time) in AgRP→PBN^{ChR2} mice (n = 5) following 40 min of laser stimulation compared to stimulation of AgRP→PBN^{GFP} mice (n = 12) (unpaired t test, p = ns).
(G) Total distance traveled in AgRP→PBN^{ChR2} mice (n = 5) with and without 30-min laser stimulation (unpaired t test, p = ns).
(H) Time spent immobile in AgRP→PBN^{ChR2} mice (n = 5) with and without 30-min laser stimulation (unpaired t test, p = ns).
(I) Acute phase formalin-induced paw licking (time) during light pulse delivery in AgRP→PBN^{GFP} mice (n = 12, paired t test, p = ns).
(J) Inflammatory phase formalin-induced paw licking (time) during light pulse delivery in AgRP→PBN^{GFP} mice (n = 12, paired t test, p = ns).
(K) Latency to paw withdrawal from 52°C hotplate during light pulse delivery in AgRP→PBN^{GFP} mice (n = 12, one-way ANOVA, p = ns).
Data are expressed as mean ± SEM, ns $p > 0.05$, *$p < 0.05$, **$p < 0.01$, ***$p < 0.001$. See also Table S2.

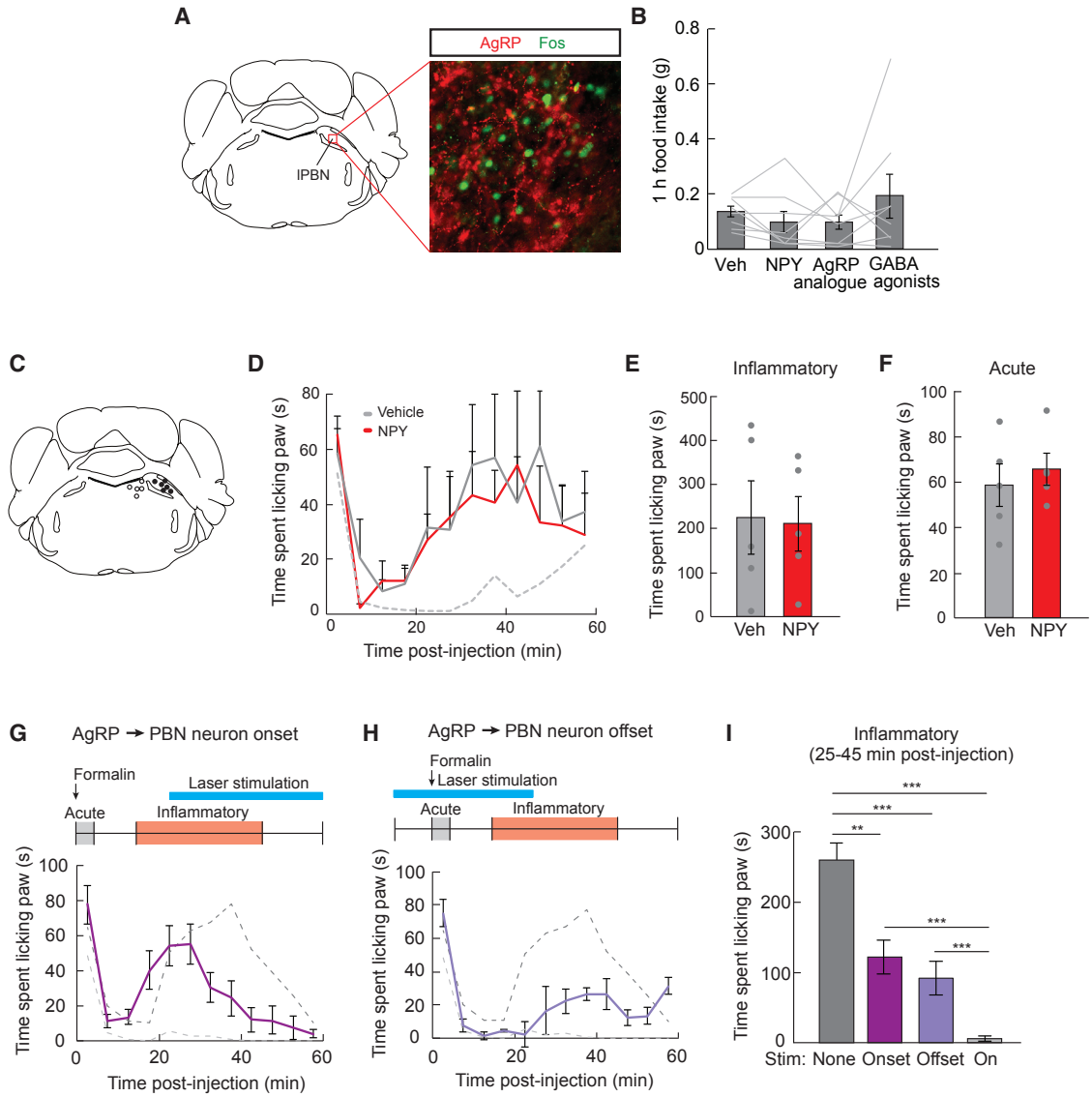

Figure S4. Peptidergic NPY Signaling in the Lateral PBN Mediates Inflammatory Phase Pain, Related to Figure 6

(A) Schematic and representative image demonstrating formalin-induced Fos and AgRP axons in the lateral PBN (lPBN).

(B) Food intake (1 h) following PBN microinjection of vehicle, NPY, an AgRP analog, or GABA agonists (n = 8, one-way repeated-measures ANOVA, p = ns).

(C) Schematic showing center of injection sites for mice injected with NPY in the lPBN (closed circles) or the locus coeruleus (LC) area (open circles).

(D) Time spent licking paw in LC vehicle- (n = 5) or NPY (n = 5) -injected mice (two-way repeated-measures ANOVA, p = ns).

(E) Inflammatory phase paw licking (time) in LC vehicle- (n = 5) or NPY (n = 5) -injected mice (unpaired t tests, p = ns).

(F) Acute phase paw licking (time) in LC vehicle- (n = 5) or NPY (n = 5) -injected mice (unpaired t tests, p = ns).

(G) Top, Experimental design: Laser stimulation was initiated 25 min post-formalin injection and lasted for the duration of the test. Bottom, graph: formalin-induced paw licking (time) with the onset of AgRP→PBN neuron activity in AgRP→PBN^{ChR2} mice (n = 12); traces of pain responses with and without AgRP→PBN^{ChR2} stimulation for the entire session are indicated in dotted lines for reference.

(H) Top, Experimental design: Laser stimulation was initiated 10 min before formalin injection and terminated 25 min post-injection. Bottom, graph: formalin-induced paw licking (time) with the offset of AgRP→PBN neuron activity in AgRP→PBN^{ChR2} mice (n = 7); traces of pain responses with and without AgRP→PBN^{ChR2} stimulation for the entire session are indicated in dotted lines for reference.

(I) Time spent responding to inflammatory pain following the onset or offset of laser stimulation (25-45 min post-injection). Inflammatory phase pain responses after the onset (magenta) and offset (purple) of AgRP→PBN^{ChR2} stimulation are compared to the inflammatory responses with and without AgRP→PBN^{ChR2} stimulation (unpaired t tests with Bonferroni correction, stimulation versus onset/offset versus no stimulation, all p values < 0.01).

Data are expressed as mean ± SEM, ns p > 0.05, t tests: **p < 0.01, ***p < 0.001. See also Table S2.

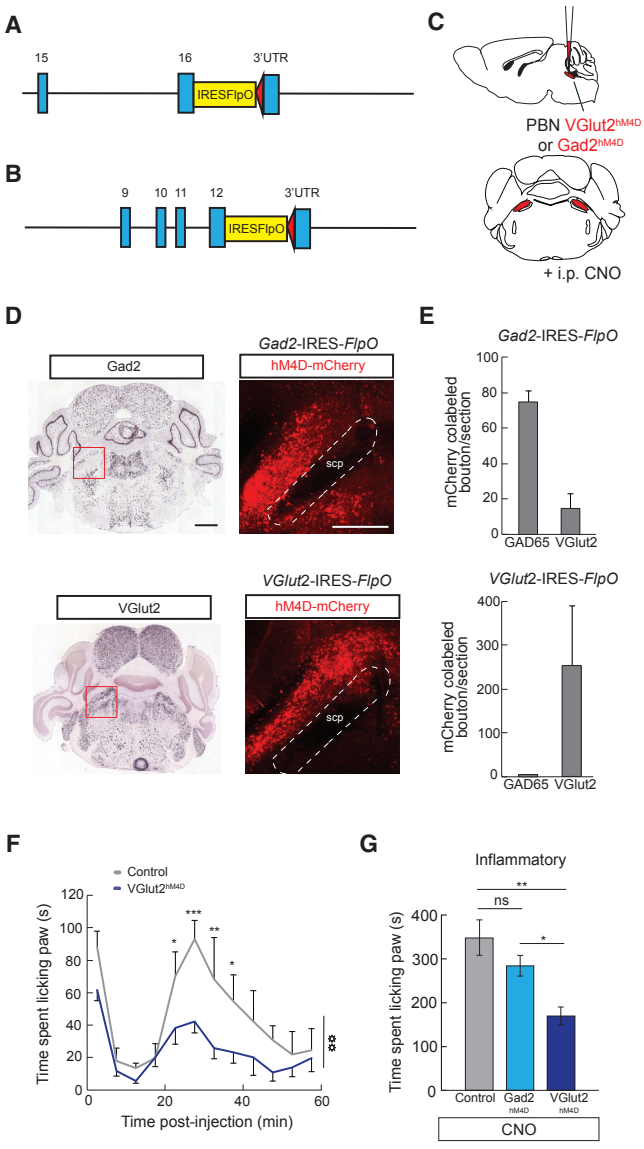

Figure S5. Glutamatergic Neurons in the lPBN Mediate Inflammatory Pain, Related to Figure 6

(A) Genomic structure of genetically modified Gad2 allele.

(B) Genomic structure of genetically modified VGlut2 allele.

(C) Strategy for expressing hM4D in Gad2 and VGlut2 PBN neurons: A FlpO-dependent rAAV expressing Cre was combined with a Cre-dependent rAAV expressing hM4D as in (Li et al., 2013), allowing for the expression of hM4D in Gad2+ and VGlut2+ lPBN neurons. These neurons were inhibited by i.p. injection of clozapine-N-oxide (CNO) as previously demonstrated (Mu et al., 2017).

(D) Left, *in situ* hybridization for Gad2 and VGlut2 mRNA in the PBN [images from Allen Brain Explorer, http://mouse.brain-map.org, (Lein et al., 2007)]. Red boxes indicated region of images to the right. Scale bar, 1 mm. Right, representative images of hM4D-mCherry expression (red) in the lPBN of experimental mice. Quantification of lPBN sections revealed an average of 98.2 ± 6.4 and 194.8 ± 35.9 hM4D-expressing neurons (per unilateral section) in *Gad2-IRES-FlpO* (n = 6) and *VGlut2-IRES-FlpO* mice, respectively. Scale bar, 500 μm. scp, superior cerebellar peduncle.

(E) Quantification of GAD65+ or VGlut2+ boutons colabeled with mCherry in *Gad2-IRES-FlpO* (top) and *VGlut2-IRES-FlpO* (bottom) mice.

(F) Time spent licking paw in control (n = 5) and VGlut2^{hM4D} (n = 6) neurons after injection of CNO (two-way repeated-measures ANOVA, main effect of group, $p < 0.01$).

(G) Inflammatory phase paw licking in control (n = 5), Gad2^{hM4D} (n = 6) Vglut2^{hM4D} (n = 6) mice following CNO injection.

Data are expressed as mean ± SEM, ns $p > 0.05$, t tests and post hoc comparisons: *$p < 0.05$, **$p < 0.01$, ***$p < 0.001$; ANOVA main effect of group: ☼☼$p < 0.01$. See also Table S2.

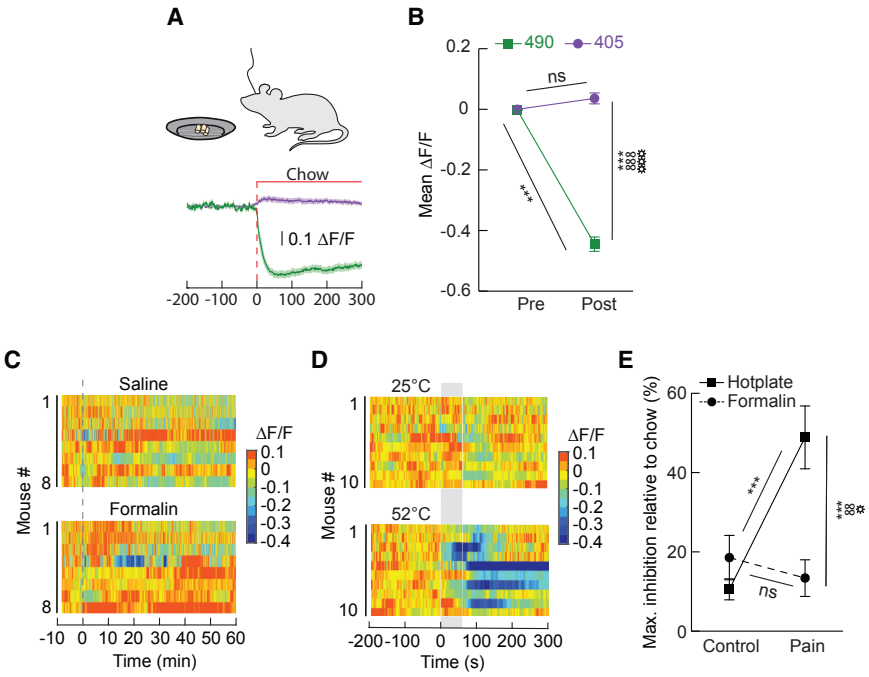

Figure S6. Acute Thermal but Not Formalin-Induced Pain Suppresses AgRP Neuron Activity, Related to Figure 7

(A) Calcium-dependent (mean, dark green; SEM, green shading) and calcium-independent (mean, dark purple; SEM, purple shading) change in fluorescence (ΔF/F) in AgRP neurons of food restricted mice (n = 10) before and after chow refeeding.

(B) Mean change in GCaMP6s signal (ΔF/F) before and after chow presentation (two-way repeated-measures ANOVA, $p < 0.001$).

(C) GCaMP6s fluorescence changes (ΔF/F) of AgRP neurons in individual mice with saline or formalin paw injection.

(D) GCaMP6s fluorescence changes (ΔF/F) in AgRP neurons of individual mice with 60 s exposure to 25°C or 52°C plate.

(E) Maximum change in AgRP neuron calcium dynamics with formalin or hotplate exposure relative to activity change observed following chow presentation (n = 10 25°C/52°C plate, n = 8 saline/formalin injection; two-way repeated-measures ANOVA, $p < 0.01$).

Data are expressed as mean ± SEM, ns $p > 0.05$, t tests and post hoc comparisons: ***$p < 0.001$; ANOVA interaction: ∞ ∞ $p < 0.01$, ∞ ∞ ∞ $p < 0.001$; ANOVA main effect of pre versus post chow presentation (B) or ANOVA main effect of condition (E): ☼$p < 0.05$, ☼☼☼$p < 0.001$. See also Table S2.